Novel determinants of NOTCH1 trafficking and signaling in breast epithelial cells

Francis M. Kobia[1,*,+], Luis Castro e Almeida[1], Francesca Carminati[1], Adrian Andronache[2], Francesco Lavezzari[1], Mark Wade[2&] and Thomas Vaccari[1,*]

[1]Dipartimento di Bioscienze, Università degli Studi di Milano, Via Giovanni Celoria, 26, 20133 Milano, Italy

[2]Center for Genomic Science of IIT@SEMM, Fondazione Istituto Italiano di Tecnologia (IIT), Milan, Italy., via Adamello 16, 20139, Milano, Italy

*Corresponding authors: Thomas Vaccari, email: thomas.vaccari@unimi.it, Francis Kobia, email: fkobia@associates.mku.ac.ke

[+]Current address: Mount Kenya University, Department of Research and Innovation, Thika, Kenya

[&]Current address: Astex Pharmaceuticals, Cambridge, UK

Abstract

The evolutionarily conserved Notch pathway controls cell–cell communication during development and in adult metazoans. It influences cell fate decisions, cell proliferation and cell differentiation, and contributes to the maintenance of normal tissue homeostasis. Consequently, misregulation of the Notch pathway is associated with a wide range of diseases, including congenital disorders and cancers with little to no cure. Signaling by Notch receptors is regulated by a complex set of cellular processes that include maturation and trafficking to the plasma membrane, endocytic uptake and sorting, lysosomal and proteasomal degradation, and ligand-dependent and independent proteolytic cleavages. We devised assays to follow quantitively the lifetime of endogenous human NOTCH1 receptor in breast epithelial cells in culture. Based on such analysis, we executed a high-content screen of 2749 human genes for which modulatory compounds exist, to identify new regulators of Notch signaling activation that might be amenable to pharmacologic intervention. We uncovered 39 new NOTCH1 genetic modulators that affect different steps of NOTCH1 cellular dynamics. In particular, we find that *PTPN23* and *HCN2* act as positive NOTCH1 regulators by promoting endocytic trafficking and NOTCH1 maturation in the Golgi apparatus, respectively, while *SGK3* serves as a negative regulator that can be modulated by pharmacologic inhibition. Our findings might be relevant in the search of new strategies to counteract pathologic Notch signaling.

Key words

Notch signaling; intracellular trafficking; Notch trafficking; cell communication

Abbreviations

ADAM: A disintegrin and metalloproteinase; ANK: Ankyrin repeats; APP: amyloid precursor protein; BafA1: Bafilomycin A1; CHX: cycloheximide; CSL: CBF1, Suppressor of Hairless, Lag-1; DAPI: 4',6-diamidino-2-phenylindole; DAPT: N-[(3,5-difluorophenyl)acetyl]-L-alanyl-2-phenyl]glycine-1,1-dimethylethyl ester; DMEM: Dulbecco's modified eagle medium; DMSO:

47 dimethyl sulfoxide; DSL: Delta/Serrate/Lag2; EDTA: ethylenediaminetetraacetic acid; EGTA:
48 ethylene glycol tetraacetic acid; EGF: epidermal growth factor; EGFR: epidermal growth factor
49 receptor; ESCRT: endosomal sorting complexes required for transport; esiRNA:
50 endoribonuclease-prepared siRNAs; ER: endoplasmic reticulum; GA: Golgi apparatus; GSI:
51 gamma (γ)-secretase inhibitor; HCS: high content screen; HCN2: hyperpolarization-activated
52 cyclic nucleotide-gated channel 2; HES1: hes family bHLH transcription factor 1; HEY1: hes
53 related family bHLH transcription factor with YRPW motif 1; HRP: horse radish peroxidase; IF:
54 immunofluorescence; KD: knockdown; MGV: mean gray value; N1FL: NOTCH1 full length;
55 N1ICD: NOTCH1 intracellular domain; ns: not significant; NT: Non-targeting; N1TM: NOTCH1
56 transmembrane; OTP: ON TARGET plus; PFA: paraformaldehyde; PM: plasma membrane;
57 pNDRG1: phospho-N-myc downstream regulated gene 1; PSENEN: presenilin enhancer gamma
58 secretase subunit; PTPN23: protein tyrosine phosphatase non-receptor type 23; RTN3: reticulon
59 3; S1: Notch cleavage site 1; S2: Notch cleavage site 2; S3: Notch cleavage site 3; SGK3:
60 serum/glucocorticoid regulated kinase family member 3; siRNA: short interfering RNA; Su(Dx):
61 supressor of deltex; TGN46: TGOLN2 (trans-golgi network protein 2); V-ATPase: vacuolar H^+
62 ATPase; w/o: washout; λ-PPA: lambda phosphatase.

63 **Introduction**

64 The evolutionarily conserved Notch pathway is a form of direct cell–cell communication
65 that is extensively deployed in the regulation of multiple cellular functions during development and
66 in adults. It influences cell fate decisions, cell proliferation and cell differentiation, and contributes
67 to the maintenance of normal tissue homeostasis in both invertebrate and vertebrate metazoans
68 [1–3]. Because of such broad function, loss or gain of Notch function is associated with several
69 congenital disorders [4] and cancers (Aster et al., 2017).

70 Upon synthesis in the endoplasmic reticulum (ER), Notch proteins are processed at site
71 S1 by Furin in the TGN (Trans Golgi Network), the distal portion of Golgi apparatus (GA). Such

72 cleavage generates the mature receptors exposed on the cell surface that are held together by
73 Ca^{2+} coordination within the heterodimerization domain (HD; see Fig. 1A for a schematic of human
74 NOTCH1) [5,6]. Once at the cell surface, Notch receptor activation can be initiated by binding the
75 Delta/Serrate/Lag2 (DSL) family of Notch ligands that are present on the surfaces of adjacent
76 signal-sending cells [7]. Following ligand binding, the receptors undergo two activating proteolytic
77 cleavages; the first one is extracellular and is executed by ADAM10 at site S2 [8]. The second is
78 intracellular and is mediated at site S3 by the γ-secretase complex [9–11] (see Fig. 1A for a
79 schematic of human NOTCH1). These cleavages generate the transcriptionally competent NICD
80 (Notch Intracellular Domain) which translocates to the nucleus and activates the expression of
81 Notch target genes [12]. In addition, Notch signaling activation may occur through non-canonical
82 means on the endosomal surface, with or without stimulation by ligands [13,14].

83 As a membrane-tethered transcription factor, the Notch signaling output is not only
84 controlled by ligands, ADAM metalloproteases, the γ-secretase complex and the CSL
85 transcriptional complex, but also through intracellular trafficking [2,12,15–18]. Indeed, loss or
86 modulation of various activities occurring at membranes positively or negatively impact signaling
87 in both model organisms and humans. These activities include glycosylation enzymes [19–21],
88 internalization regulators such as Dynamin [22], and ubiquitin ligases such as Dx (Deltex) [23–
89 27], Su(Dx) (suppressor of Deltex)/AIP4/ITCH in mammals [28,29], and NEDD4 [17,30]. In
90 addition, components of the endo-lysosomal system, such as Endosomal Sorting Required for
91 Transport (ESCRT) proteins [31–33] or the vacuolar-ATPase (V-ATPase) pump are required for
92 endocytic Notch trafficking and signaling [34–40]. It is plausible that numerous other factors, yet
93 to be identified and characterized, contribute to fine tune Notch liberation from membranes
94 signaling by harnessing the intracellular trafficking machinery. Thus, aiming to improve knowledge
95 of Notch receptor trafficking and to identify novel genes that control Notch trafficking and
96 signaling, here we combine quantitative immunofluorescence, RNA interference, and automated
97 microscopic imaging to describe the kinetics of endogenous NOTCH1 export to the plasma

98 membrane (PM), and its endocytic uptake and lysosomal clearance in human epithelial mammary
99 gland cells in culture. Finally, we screen to identify novel modulators of Notch trafficking and
100 signaling.

101 **Materials and methods**

102 **Cell culture**

103 MCF10A cells (ATCC, Cat #: CRL-10317) were cultured in DMEM/F12 (ThermoFisher
104 Scientific, Cat #: 11320033) supplemented with 5% Horse Serum (ThermoFisher Scientific, Cat
105 #: 16050122), 10 mg/ml insulin (Merck Life Sciences, Cat #: 11376497001), 0.5 mg/ml
106 Hydrocortisone (Merck Life Sciences, Cat #: H0888-5G), 100 ng/ml cholera toxin (Merck Life
107 Sciences, Cat #: C8052-2MG) and freshly added 20 ng/ml EGF (Vinci-Biochem, Cat #: 90201-3).
108 The MCF10A-RbpJk-Luc Notch signaling reporter cell line, which carries a luciferase gene under
109 the control of a Notch promoter, was maintained under antibiotic selection in normal MCF10A
110 medium supplemented with puromycin (Vinci-Biochem, Cat #: AG-CN2-0078-M100) at a final
111 concentration of 2 mg/ml.

112 **Compounds and chemicals**

113 Where indicated, cells were treated with the following compounds and/or chemicals at
114 indicated concentrations. γ-secretase inhibitor: DAPT (Santa Cruz Biotechnology, Cat #: sc-
115 201315), V-ATPase inhibitor: BafA1 (Santa Cruz Biotechnology, Cat #: sc-201550), SGK3
116 inhibitor: VPS34-IN1 (Selleckchem, Cat #: S7980). Stock solutions of the compounds were
117 prepared in cell culture grade DMSO (EuroClone, Cat #: EMR385250). λ-phosphatase (λ-PPA)
118 along with 10X λ-PPA reaction buffer and 10X $MnCl_2$) was purchased from Santa Cruz
119 Biotechnology (Cat #: sc-200312A). EGTA was purchased from Santa Cruz Biotechnology (Cat
120 #: sc-3593D).
121

122 **EGTA stimulation of Notch cleavage, nuclear translocation and signaling**

123 Notch signaling activation was stimulated by Ca^{2+} depletion [6]. For short-term Ca^{2+}
124 removal, EGTA was added at a final concentration of 10mM for up to 30 minutes, while for
125 extended periods, EGTA was used at a final concentration of 2.5mM for 2–4 hours, followed by
126 downstream assays.

127 **Immunofluorescence**

128 Immunofluorescence (IF) was performed on cells grown on coverslips. For IF staining,
129 cells were fixed for 10 minutes with 4% PFA at room temperature. They were then rinsed thrice
130 with PBS 1X and then permeabilized for 10 minutes with 0.1% triton-PBS 1X or with 0.01%
131 saponin in PBS. They were then incubated in 3% BSA in PBS 1X blocking solution or in 0.01%
132 saponin in PBS for 30 minutes and then incubated with primary antibody dissolved in the
133 appropriate blocking solution for 1 hour at room temperature. Excess antibody was washed off by
134 rinsing 3 times with PBS 1X, 5 minutes each. Samples were then incubated in secondary antibody
135 diluted in the appropriate blocking solution for 1 hour at room temperature followed by 3 washes
136 using PBS 1X, 5 minutes per wash. The following primary antibodies were used: rat anti-full length
137 NOTCH1, 5B5 monoclonal antibody (Merck Life Sciences, Cat #: SAB4200024) at 1:300, Goat
138 anti-EEA1 (Santa Cruz, Cat #: sc-6415) at 1:150, Rabbit anti-GIANTIN (Covance, Cat #: PRB-
139 114C) at 1:1000, mouse anti-EGFR 108 (hybridoma, ATCC) at 1:500, rabbit anti-Reticulon3
140 (RTN3; generous gift from Dr. Sara Sigismund, IEO, Milan) at 1:300, rabbit anti-TGN46
141 (Proteintech, Cat #:13573-1-AP) at 1:300, and rabbit anti-LAMP1 (Merck Life Sciences, Cat #:
142 L1418) at 1:200 (requires permeabilization with saponin). Cell surface membranes were marked
143 with phalloidin (Merck Life Sciences, Cat #: P5282) at 1:100 and the nuclei counterstained with
144 DAPI (Merck Life Sciences, Cat #: D9542) at 1:1000. Confocal image acquisition was done using
145 a Leica TCS SL confocal system. Where noted, digital images were processed using Photoshop
146 or ImageJ software without biased manipulation.

147 ImageJ was used for quantitative analysis of IF images following spatial image calibration
148 based on imaging scale bars. To assess colocalization in co-stained samples, imaging channels
149 were first separated using the split channel function of ImageJ. To quantify NOTCH1
150 accumulation in the Golgi in HCN2- and SGK3-silenced conditions, and the accumulation of
151 NOTCH1 and EGFR in the Golgi and endoplasmic reticulum (ER) upon EGTA treatment,
152 ImageJ's freehand selection tool was used to trace regions of interest (ROIs) based on Giantin,
153 TGN46, or RTN3 signals. The ROIs were then saved and transferred onto the NOTCH1 and
154 EGFR channels using the ROI manager tool. Next, the areas (μm^2) and integrated densities
155 (IntDens) of the ROIs were measured to determine organelle (GA) size and the signal intensities
156 of NOTCH1 and EGFR (in the GA and ER), respectively. To quantify the levels of NOTCH1 and
157 EGFR at the PM, ImageJ's freehand tool was used to mark ROIs covering the area between the
158 inner and outer sides of the PM based on the NOTCH1 and EGFR cell surface signal. The IntDens
159 within the ROIs was then measured to determine NOTCH1 and EGFR levels at the PM. To
160 measure whole cell levels of NOTCH1/EGFR, whole-cell ROIs were created by tracing the outer
161 side of the PM based on the NOTCH1 and EGFR signals, followed by IntDens measurement to
162 determine the levels of NOTCH1 and EGFR in whole cells. The proportions (%) of NOTCH1 and
163 EGFR in each compartment were determined by applying the following formula in their respective
164 channels: % IntDens = (ROI IntDens ÷ whole cell ROI IntDens) × 100. At least 5 ROIs, in at least
165 five images were analyzed. The number of endolysosomal puncta, NOTCH1- and EGFR-positive
166 puncta, and the rate of NOTCH1 colocalization with EEA1 (early endosomes) and LAMP1 (late
167 endosomes/lysosomes) in *PTPN23*- and *SGK3*-silenced samples, as well as the rate of NOTCH1
168 and EGFR colocalization with LAMP1 in Bafilomycin (BafA1)-treated cells were determined as
169 follows. First, ImageJ's freehand tool was used to trace the cytoplasmic area between the edge
170 of the nucleus and the inner side of the PM on merged (NOTCH1+DAPI+EEA1,
171 NOTCH1+DAPI+LAMP1, or EGFR+DAPI+LAMP1) composite images. The ROIs were then
172 saved and transferred onto the respective single channels using the ROI manager tool. The

173 number of NOTCH1-, EGFR-, EEA1-, or LAMP1-positive puncta was then determined using
174 ImageJ's ComDet v.0.5.5 plugin (DOI: https://doi.org/10.5281/zenodo.6546038) after empirically
175 determining the spot detection thresholds for each channel. For spot (puncta) detection, the
176 intensity threshold was set at 4 and colocalization determined using a maximum distance of 2
177 pixels between colocalized spots. To determine the rate of colocalization with the organelle
178 markers, the NOTCH1 or EGFR channels were merged the EEA1 or LAMP1 channels to generate
179 composite images and the ComDet plugin used to determine the rate of puncta colocalization. At
180 least 5 ROIs, in at least 5 images were analyzed.

181 **Western blot analyses**

182 For western blot analyses, cells were scraped into 1 ml of the media they had been
183 cultured in, transferred into prechilled 1.5 ml Eppendorf tubes, and placed on ice. They were then
184 centrifuged at full speed (14,000 rpm) for 5 minutes at 4°C and the pellets rinsed once with ice-
185 cold PBS 1X. Unless indicated otherwise, cell pellets were then lysed by resuspension in 60 µl
186 ice-cold RIPA buffer (ThermoFisher Scientific, Cat. #: 89901) supplemented with a protease
187 inhibitor cocktail (Merck Life Sciences, Cat #: 11697498001). They were then vortexed for 10
188 seconds, incubated on ice for 15 minutes, cleared by centrifugation at full speed for 20 minutes
189 at 4°C, and the supernatants transferred into fresh 1.5 ml Eppendorf tubes on ice. Protein
190 concentrations were quantified using a BCA protein assay kit (ThermoFisher Scientific, Cat #:
191 233225) following manufacturer guidelines. Next, for each sample, 20 µg of the protein lysate
192 were mixed with 7.5 µl of 4X Laemmli sample buffer (Bio-Rad Laboratories, Cat #: 1610747)
193 containing 10% β-mercaptoethanol (Bio-Rad, Cat #: 1610710) and the volume topped up to 30 µl
194 using distilled water. Depending on target protein molecular weight, the samples were then
195 resolved on precast 4–20% Criterion™ TGX Stain-Free™ polyacrylamide gels (Bio-Rad, Cat #:
196 5678094) or 7.5% stain-free gels (Bio-Rad, Cat #: 4568024 or 5678024) polyacrylamide gels
197 using 1X Tris/Glycine SDS running buffer (Bio-Rad, Cat #: 1610732). Proteins were then

198 transferred onto 0.2 μm nitrocellulose membranes using Trans-Blot® Turbo™ Mini Nitrocellulose
199 Transfer Packs (Bio-Rad, Cat #: 1704158EDU) on a Trans-Blot Turbo TM Transfer System (Bio-
200 Rad, Cat #: 1704150). Protein transfer was then visualized using 0.1 % Ponceau S solution (w/v)
201 in 5% acetic acid (Merck Life Sciences, Cat #: P7170-1L) and imaged. The membranes were then
202 washed using 1X TBS (Bio-Rad, Cat #: 1706435) containing 0.1% Tween-20 (Bio-Rad, Cat #:
203 1610781) – TBST, for 15 minutes and then blocked with 5% skimmed milk (Merck Millipore, Cat
204 #: 70166) in TBST for 3 hours. Membranes were then incubated overnight at 4°C in the following
205 primary antibodies: rabbit anti-cleaved NOTCH1 (Val 1744) at 1:1000 (Cell signaling technology,
206 Cat #: 4147S), rabbit anti-NOTCH1 (D1E11) XP® at 1:1000 (Cell signaling technology, Cat #:
207 3608S), mouse anti-Vinculin at 1:5000 (Bio-Rad, Cat #: MCA4665GA), mouse anti-β-actin at
208 1:5000 (Merck Life Science, Cat #: A-5441), or rabbit anti-Phospho-NDRG1 (Thr346) (D98G11)
209 XP® at 1:1000 (Cell signaling technology, Cat #: 5482). Membranes were then washed thrice with
210 TBST (5 minutes/wash) at room temperature and then incubated with HRP-conjugated goat anti-
211 rabbit IgG (H + L) (Bio-Rad, Cat #: 170-6515) or goat anti-mouse IgG (H + L) (Bio-Rad, Cat #: 170-
212 6516), both at 1:5000, for one hour at room temperature. They were then washed thrice with
213 TBST (5 minutes/wash) at room temperature and signal developed for one minute using Clarity™
214 Western ECL substrate (Bio-Rad, Cat #: 1705060) or Clarity Max Western ECL Substrate (Bio-
215 Rad, Cat #: 1705062). They were then imaged on a ChemiDoc MP imaging system (Bio-Rad).
216 Band intensities were quantified using Image Lab software (Bio-Rad) followed by statistical
217 analysis and graph visualization using GraphPad Prism.

218 **Lambda phosphatase (λ-PPA) treatment**

219 For the λ-PPA assay, two types of RIPA lysis buffer were used – RIPA supplemented with
220 protease (phenylmethylsulfonyl fluoride and 1 tablet of 1X cOmplete mini protease inhibitor
221 cocktail, EDTA-free) and phosphatase (sodium fluoride and sulfur monoxide) inhibitors, and RIPA
222 supplemented with protease inhibitors only (phenylmethylsulfonyl fluoride and 1 tablet of 1X

223 cOmplete mini protease inhibitor cocktail, EDTA-free). The first lysis buffer (containing
224 phosphatase inhibitors) was used as a negative control for phosphatase treatment. MCF10A cells
225 were harvested, lysed in the appropriate ice-cold RIPA buffer (with or without phosphatase
226 inhibitor), and protein quantified as described in section 2.5. Next, for each sample (protein
227 concentration: 1 μg/μl), 25 μg of protein (25 μl) were subjected to λ-PPA treatment following
228 manufacturer instructions. Briefly, 0.5 μl of λ-PPA (20,000 U) were added into each tube
229 (containing 25 μl of the sample), along with 3.2 μl of 10X λ-PPA buffer and 3.2 μl of 10X $MnCl_2$
230 (final volume: 32 μl). The samples were then mixed by gently flicking the tube and incubated for
231 30 minutes at 30°C. Next, 10.75 μl of 4X Laemmli loading buffer were added into each sample,
232 followed by western blotting using the antibody against the γ-secretase-cleaved (Val1744)
233 NOTCH1 intracellular domain (N1ICD).

234 **Cycloheximide treatment and assessment of NOTCH1 protein stability**

235 Where indicated, after gene knockdown for 72 hours, MCF10A cells were treated with 10
236 μM cycloheximide (CHX) to block protein synthesis or an equal volume of DMSO (vehicle) for 4
237 hours. Cells were then harvested, lysed, and protein concentration quantified as described in
238 section 2.5. To assess NOTCH1 protein stability, 20μg of the protein lysate per sample were
239 subjected to western blot analysis using the antibody against full length NOTCH1 (N1FL) and
240 transmembrane NOTCH1 (N1TM), as well as the antibody against the γ-secretase-cleaved
241 N1ICD. Band intensities were then analyzed on GraphPad Prism to determine the differences
242 between the levels of N1FL, N1TM, and N1ICD in the CHX-treated vs untreated cells.

243 **Gene silencing**

244 Gene knockdowns were performed in 384-well plate format. Each gene/well was targeted
245 with a pool of four distinct siRNAs against different sequences of the respective target transcript.
246 Each of the 10 libraries was knocked down in 6 replicates. Three of the replicates were subjected
247 to EGTA stimulation while the other 3 were left unstimulated. For siRNA transfection, cells were

248 always maintained at less than 6 passages and trypsinized for transfection while at 60%–80%
249 confluence. All siRNA transfections were done in black 384-well, tissue culture treated optical
250 plates (Corning, Cat #: 3712), using the reverse transfection method. Briefly, desired siRNAs were
251 diluted in Optimem (ThermoFisher Scientific, Cat #: 51985-042) at a concentration of 50 nM,
252 complexed with 0.12 µl of Lipofectamine™ RNAiMAX Transfection Reagent (ThermoFisher
253 Scientific, Cat #: 13778500) per 20 µl of Optimem-siRNA solution for 20 minutes at room
254 temperature, and 20 µl of the complex dispensed into each 384 well. Where indicated, esiRNA
255 was used at a final concentration of 50 nM. Cells were suspended at a density of 35 cells/µl in 2X
256 MCF10A cell culture media and 20 µl of the cell suspension (700 cells) added into each well
257 (containing 20 µl of the transfection complex) to obtain a final siRNA concentration of 25 nM. The
258 2X medium was prepared using each component of the medium at double its standard
259 concentration. Double the concentration of EGF shown in section 2.1 was added fresh into the
260 cells before they were added into the wells. Cells were then cultured for 72 hours as described in
261 section 2.1, in a SteriStore™ automated incubator (HighRes Biosolutions). All solutions were
262 dispensed using the Freedom EVO automated liquid handler system (Tecan).

263 To stimulate NOTCH1 activation, at the end of the 72 hours of gene knockdown, 3 plates
264 from each library were treated with EGTA for 2 hours to stimulate Notch cleavage. To do this, 10
265 µl of fresh media containing 12.5 mM EGTA was directly added into the wells to a final
266 concentration of 2.5 mM EGTA per well, and a final volume of 50 µl/well. The NoEGTA stimulation
267 plates received 10 µl of sterile water. The plates were then incubated for 2 hours at 37°C and
268 then fixed with 2% PFA for 15 minutes at room temperature. Fixation was done by adding 50 µl
269 of 4% PFA directly into the wells. Solutions were dispensed into the wells using a Multidrop™
270 Combi Reagent Dispenser (ThermoFisher Scientific).

271 **Automated immunofluorescence analyses**

272 Automated immunostaining for high content screening (HCS) was performed using a
273 Biotek EL406 washer/dispenser equipped with a 192-tube aspiration manifold. The solution was
274 removed from the wells and the cells rinsed once with 1X PBS. Cells were permeabilized with
275 0.05% triton in 1% BSA blocking solution for 1 hour at room temperature followed by a single
276 wash with 1X PBS. Cells were then incubated for 1 hour at room temperature with the anti-
277 NOTCH1 primary antibody (Merck Life Sciences, Cat #: SAB4200024) diluted at 1:350 in 1% BSA
278 blocking solution. The primary antibody solution was then removed, and the plates washed twice
279 with 1X PBS. Next, the cells were incubated for 1 hour with 1% BSA blocking solution containing
280 DAPI at 1:4,500 (Merck Life Sciences, Cat #: D9542), phalloidin at 1:350 (Merck Life Sciences,
281 Cat #: P5282), and Alexa Fluor 488 anti-rat secondary antibody at 1:400 (ThermoFisher Scientific,
282 Cat #: A21208). They were then washed thrice with 1X PBS before imaging. Where imaging could
283 not be performed immediately, the immunostained cells were stored at 4°C for not more than 48
284 hours prior to image acquisition.

285 **Automated image acquisition**

286 The 384-well plates were scanned using an automated Olympus Scan^R (Tokyo, Japan)
287 microscope equipped with a Hamilton arm for plate handling. Eight fields of view and three
288 emission fluorescent channels (DAPI, phalloidin, and Alexa 488), were acquired for each well
289 using a 20X objective. Imaging data were annotated and transferred to the Isilon infrastructure
290 and network software and indexed by plate barcode for storage. In the annotation each well was
291 assigned information regarding the date of the experiment, the gene knocked down, the sub-
292 genomic library the knocked down gene belongs to, and the treatment (EGTA vs NoEGTA).
293 Images were then uploaded to the Columbus server (PerkinElmer), where they could be accessed
294 for visual examination and automated analysis.

295 **High content screen image analysis**

296 An in-house Acapella (PerkinElmer) image analysis script was developed and used for
297 batch image analysis and to quantitatively describe a set of phenotypic features. All analyzed
298 images were first subjected to background correction and exclusion of unevenly illuminated
299 images. Background correction was done separately for each channel. DAPI, which was used to
300 mask the nuclei and phalloidin, which labeled cell surfaces, were used for cell segmentation.
301 Segmentation was performed using a modified version of the watershed algorithm, which allowed
302 the inversion of phalloidin channel images so as to display high pixel intensities in the cell and
303 low intensities along the cell membrane, allowing application of the watershed approach to identify
304 cell boundaries. This algorithm also detects and excludes regions of the image fields not covered
305 by cells. Once the cells, their membranes, and corresponding nuclei were detected, each cell was
306 segmented into the nucleus based on DAPI staining, the membrane based on phalloidin signal,
307 and the cytosol (region between the nuclei and cell surface membrane). Cells that were adjacent
308 to field of view borders, those deemed to be too small or too big, those with saturated pixel
309 intensities or those that were improperly segmented, were excluded from downstream image
310 analysis. To exclude out-of-focus images, we used boxplot statistics on the distribution of intensity
311 contrast values (on the DAPI channel) of all nuclei detected in the entire well. Using the first and
312 the third quantiles of this distribution, we estimated the lower inferior fence (LIF) using the 95%
313 confidence interval. For each field of view, we next established the number of nuclei presenting a
314 contrast lower than the LIF and classified fields in which >50% of the nuclei failed to cross the LIF
315 threshold as being out of focus. Data analysis on the EGTA stimulated plates was performed
316 independently of the corresponding non EGTA-treated plates. For each gene (well), the
317 parameters of interest were quantified and reported as z-score values [41].

318 **Candidate gene selection for validation**

319 For each library plate, candidate genes from the EGTA and the NoEGTA conditions were
320 considered to affect respective parameters if their knockdown shifted the z-score positively or

321 negatively, the further the shift, the stronger the phenotype. The main parameters quantified were,
322 a) cell viability (QC1_NoOfAnalysedCells), b) Overall Notch intensity in the cell (N4_CellNotch),
323 c) nuclear Notch intensity (N1_NucNotch), d) cell surface membrane Notch intensity
324 (N3_MembNotch), and e) Notch accumulation in intracellular compartments
325 (N5_PercentOfCellsWithSpots & N9_NoOfSpotsPerCell).

326 **Generation of the stable Notch signaling reporter cell line, MCF10A-RbpJk-Luc**

327 A Notch pathway transcriptional output reporter cell line was generated by infecting
328 MCF10A cells with Cignal Lenti RBP-Jk Reporter (luc) lentiviral particles (Qiagen, Cat #: CLS-
329 014L) following manufacturer instructions. This reporter system carries an inducible RBP-Jk-
330 responsive firefly luciferase reporter as well as a puromycin resistance gene that permits the
331 selection of cells that stably integrate the reporter construct. To isolate stably infected single cell
332 clones, the cells were counted and serially diluted in order to have a final concentration of 2.5
333 cells/ml. Next, 200µl of the cell suspension were seeded onto four 96-well plates so as to have
334 0.5 cells/well. The cell culture medium was changed twice a week and in the second week the
335 cells were examined for single cell clones. Each of the healthiest looking clones, but with a slightly
336 different cell morphology relative to normal MCF10A cells were selected, transferred onto 48-well
337 plates, grown while observing the growth characteristics, and then transferred into 6-well plates
338 after reaching 70%–80% confluence. Eventually each single cell clone population was split into
339 two wells of a 6-well plate and frozen after reaching 70%–80% confluence, followed by long term
340 storage in liquid nitrogen. Each clone was then tested using a luciferase assay for Notch signaling
341 inducibility using EGTA. The two best clones with the widest Notch signaling induction assay
342 window, measured as the ratio between basal luciferase activity (in the absence of EGTA) to
343 activated luciferase activity (in the presence of EGTA), clone 1 and clone 13, were selected for
344 further characterization.

345 To assess the ability to activate and control the Notch pathway in the stable Notch reporter
346 cell lines, MCF10A-RbpJk-Luc single cell clones were seeded on white, opaque, flat-bottomed 96
347 well plates (Merck Life Sciences, Cat #: CLS3362-100EA) at 9,000 cells, in 100 µl of medium and
348 grown overnight. Notch signaling was then stimulated by adding 11 µl of media supplemented
349 with 25 mM EGTA into each well to reach a final concentration of 2.5 mM EGTA in 111 µl of
350 medium. The cells were then incubated with EGTA for 2 hours to allow Notch signaling activation
351 and resulting luciferase synthesis. The luciferase assay was then performed by adding 9 µl of
352 fresh medium containing 6.6 mM of D-luciferin into each well to have a final concentration of 500
353 µM D-luciferin per well, in a final volume of 120 µl per well. The cells were then incubated for 2
354 hours after which luminescence readings were taken on a Promega Glomax multimode plate
355 reader. To assess the ability to block Notch signaling activation in the reporter cell line, we
356 silenced *NOTCH1*, *PSENEN,* and *ADAM10* for 72 hours using siRNA (Dharmacon) before Notch
357 signaling activation and the luciferase assay. To account for reductions in cell proliferation upon
358 gene silencing, a cell viability assay was performed after the luciferase assay by adding 12 µL of
359 resazurin (Merck Life Sciences, Cat #: TOX8-1KT) and the cells incubated for an additional 2
360 hours followed by fluorescence reading on a Promega Glomax multimode plate reader.

361 **Secondary screen for signaling activity**

362 Relevant genes were knocked down in MCF10A-RbpJK-Luc Notch signaling reporter
363 cells, on white opaque 384-well plates (Corning, Cat #: 3712) followed by luciferase/proliferation
364 assays using 500 µM D-luciferin and 2.5% resazurin after 72 hours. Where indicated EGTA was
365 used at a final concentration of 2.5 mM. Briefly, a mix of D-luciferin+resazurin was prepared
366 immediately before the experiment by dissolving D-luciferin and resazurin in normal MCF10A
367 cells media at a concentration 3.6X higher than the desired final concentration. Where EGTA-
368 stimulated Notch activation was desired, a mix of D-luciferin+resazurin+EGTA was prepared by
369 including EGTA at a concentration 3.6X higher than its desired final concentration. Next, 15 µl of

370 the appropriate solution of Notch luciferase assay mix was added into each well of the 384-well
371 plate and the cells incubated for 4 hours in normal conditions. To assess Notch signaling output
372 (luminescence) and cell viability (resazurin fluorescence), luminescence and fluorescence were
373 read on a PHERAstar BMG LABTECH microplate reader.

374 **Statistical analyses**

375 All experimental data were analyzed on GraphPad Prism. All data represent at least 3
376 independent replicates and are shown in graphs as individual values, mean ± SD, or normalized
377 values. Statistical differences between two groups were evaluated using unpaired two-tailed
378 Student's t-tests, with *, **, ***, ****, and ns indicating $p < 0.05$, $p < 0.01$, $p < 0.001$, $p < 0.0001$, and
379 not significant, respectively. Data and statistical analyses for the screen were done as described
380 in section 2.11.

381 **Acknowledgements and funding information**

382 We thank Fernanda Ricci and Michela Mattioli for excellent technical help during the
383 execution of the HCS. This work is supported by AIRC (Associazione Italiana Ricerca sul Cancro)
384 IG grant 20661 and WCR (Worldwide Cancer Research) Grant 18-399 to TV and by IIT@SEMM.

385 **Author contributions**

386 FMK and TV designed the study. FMK, LCA, FC and FL conducted the experiments. AA
387 performed the computational analyses of the screening data. MW coordinated the execution of
388 the HCS screen. TV wrote the manuscript with the help of FMK and LCA.

389 **Results**

390 **Canonical NOTCH1 signaling in human MCF10A cells**

391 Knowledge about Notch signaling dynamics is a prerequisite to investigating factors that
392 control signaling by modulating its trafficking to subcellular compartments. MCF10A cells, derived
393 from non-transformed human breast epithelial cells [42], express Notch signaling pathway ligands

394 and receptors including *NOTCH1*, *NOTCH2*, and *NOTCH3*, while *NOTCH4* is not detectable [34].
395 Immuno-localization with an antibody that recognizes the intracellular domain of NOTCH1, shows
396 that endogenous NOTCH1 is localized on the cell surface of confluent MCF10A cells (Fig. 1B).
397 As expected, efficient knockdown (KD) of key components of the Notch signaling pathway, such
398 as *ADAM10* (encoding the S2 cleavage metalloprotease) and *PSENEN* (encoding a γ-secretase
399 component necessary for S3 cleavage) in MCF10A cells prevented the translocation of
400 endogenous NOTCH1 into the nucleus upon EGTA-mediated Ca^{2+} chelation (Fig. 1B–C;
401 materials and methods). Consistent with this, *NOTCH1*, *ADAM10* or *PSENEN* depletion
402 significantly suppressed EGTA-stimulated Notch signaling, when measured in MCF10A cells
403 stably expressing the Notch activation reporter RBPj-luc (Fig. 1D).

404 We previously observed that the S3-cleaved NOTCH1 intracellular domain (N1ICD) is
405 visible in western blots as a band doublet around the 120 kDa region [34] (Fig. 1E). We suspected
406 that the slightly higher molecular weight band of the doublet may represent the N1ICD that is
407 phosphorylated and destined for proteasomal degradation, while the lower molecular weight band
408 represents newly generated N1ICD that has not been phosphorylated [43–45]. Indeed, in extracts
409 of cells treated with the γ-secretase inhibitor DAPT to block the production of N1ICD, we observed
410 the presence of the upper band only (Fig. 1E). To test if the upper band of the N1ICD doublet was
411 indeed phosphorylated, we harvested proteins from unstimulated MCF10A cells, or from cells
412 stimulated with EGTA for 10 minutes to induce N1ICD generation, or from cells stimulated with
413 EGTA for 10 minutes and then returned to normal medium for 1.5 hours. We then treated the
414 lysates with or without λ-phosphatase (λ-PPA) [46]. λ-PPA treatment resulted in a minor downshift
415 of the N1ICD in extracts stimulated with EGTA for 10 minutes and in a large downshift in those in
416 which the EGTA had been washed out for 1.5 hours after stimulation, indicating that N1ICD is
417 progressively phosphorylated shortly after S3 cleavage (Fig. 1F). Together, these data indicate
418 that MCF10A cells are endowed with an endogenous pool of plasma membrane-localized

419 NOTCH1 that can be canonically activated in a S2 and S3-dependent fashion to promote target
420 gene transcription before being phosphorylated.

421 **Dynamics of NOTCH1 receptor trafficking in MCF10A cells**

422 To study the dynamics of endogenous NOTCH1 trafficking, we first treated MCF10A cells
423 with the V-ATPase inhibitor BAfA1 for 4 hours to block lysosomal protein degradation. As
424 previously observed [34], while most of NOTCH1 is localized to the plasma membrane (PM) in
425 control-treated cells, NOTCH1 accumulates in an slightly expanded LAMP1-positive lysosomal
426 compartments in BafA1-treated cells. A similar pattern of localization is observed for EGFR (Fig.
427 2A, quantified in A'). These data indicate that in unstimulated conditions endogenous NOTCH1
428 localization represents the steady state of a receptor that is continuously trafficked to lysosomes
429 for degradation.

430 Because new synthesis of NOTCH1 is expected to compensate for its rapid lysosomal
431 degradation, we studied NOTCH1 exocytic trafficking relative to EGFR. Consistent with
432 continuous secretory trafficking of newly synthesized NOTCH1, we observe that in untreated cells
433 an intracellular pool of NOTCH1 and EGFR colocalizes with the endoplasmic reticulum marker
434 RTN3 (Reticulon-3; Fig. 2B). We reasoned that Ca^{2+} chelation, in addition to triggering shedding
435 of the extracellular portion of Notch, when prolonged, is known to lead to exhaustion of the
436 intracellular Ca^{2+} stores and membrane fusion arrest [47,48]. Indeed, 4 hours treatment with
437 2.5mM EGTA results in clearing of the PM of existing NOTCH1 molecules and to accumulation
438 of most NOTCH1 and EGFR in a RTN3-positive compartment (Fig. 2B; note that EGFR is still
439 visible at the cell surface). This experiment highlights a strategy for controlling the release of
440 NOTCH1 and tracking its trafficking to the PM.

441 To time endogenous NOTCH1 and EGFR trafficking from the ER to the cell surface, we
442 washed out the EGTA-containing media after the 4-hour treatment with fresh complete medium
443 (w/o). We then subjected the cells to immunolabeling for NOTCH1, EGFR, and Giantin, a marker

444 of the Golgi apparatus (GA). Interestingly, we observe that an intracellular pool of NOTCH1 and
445 EGFR colocalizes with Giantin. Treating the cells with EGTA for 4 hours caused accumulation of
446 most NOTCH1, EGFR in the ER, as well as alteration of Giantin localization (Fig. 2C, quantified
447 in C'). Strikingly, both NOTCH1 and EGFR almost exclusively localized in the GA upon 1 hour
448 w/o, indicating that NOTCH1 and EGFR trafficking is rapidly resumed after EGTA w/. A 4-hour
449 w/o fully restored NOTCH1 localization to the GA, while EGFR localization to the GA did not
450 normalize. In contrast, A 4-hour w/o fully restored EGFR localization to the cell surface, while that
451 of NOTCH1 required longer (Fig. 2C, quantified in C'). These data reveal time-resolved kinetics
452 of NOTCH1 and EGFR secretion from the ER to the GA, and to the PM, and indicate that the bulk
453 of the NOTCH1 pool progresses from the ER to GA and from GA to the cell surface in about 4
454 hours. Slight differences between trafficking of NOTCH1 and EGFR suggest that the two
455 receptors might possess distinct trafficking and processing requirements. Our analyses of the
456 timing of endogenous NOTCH1 and EGFR secretory trafficking are consistent with the timing of
457 endocytic degradation obtained by limiting lysosomal activity with BafA1 treatment and suggest
458 that in MCF10A cells NOTCH1 and EGFR molecules possess a limited lifespan of about 8 hours.

459 **High-content screening identifies 51 novel potential modulators of intracellular NOTCH1**
460 **localization**

461 The limited lifespan of endogenous NOTCH1 in MCF10A cells predicts that perturbation
462 of genes that control NOTCH1 steady state localization might significantly alter signaling. Thus,
463 we tested whether the activity of 2749 human genes with known or predicted small compound
464 inhibitors belonging to different functional categories (see Supplemental file 1) is required for
465 correct NOTCH1 localization in MCF10A cells. To this end, we reverse transfected cells on 10
466 arrayed plates containing individual pools of silencing RNAs (siRNA) targeting the human genes
467 and controls in unstimulated cells (Fig. 3A). To identify genes that are also important for NOTCH1
468 nuclear localization upon signaling activation, we subjected duplicate plates to EGTA stimulation.

469 We then stained cells with an antibody that recognizes the cytoplasmic portion of NOTCH1. The
470 cells were counterstained with DAPI and phalloidin to visualize nuclei and cell cortices,
471 respectively (Fig. 3B). We devised an automated high content image analysis pipeline to identify
472 factors that when silenced affected NOTCH1 subcellular localization by altering receptor amounts
473 on the cell surface, in the cytoplasm, or in the nucleus (Fig 3B). In such primary screen, we
474 identified 231 potential modulators of NOTCH1 localization (Fig. 4A; Supplemental File 2). We
475 then retested the positive hits using a custom-made plate containing 231 pools of esiRNA, a gene-
476 silencing reagent comprised of a heterogeneous mixture of numerous siRNA targeting each gene
477 [49] identified in the primary screen. This validation screen yielded 73 hits (Fig. 4B). Only 51 of
478 them confirmed the effects observed in the primary screen. Of these, the majority (44/51)
479 increased the intracellular pool of NOTCH1 either in unstimulated (NoEGTA, 36 hits) or in
480 stimulated conditions (+EGTA, 8 hits), while a minority altered both PM and intracellular NOTCH1
481 or increased nuclear NOTCH1 (Fig. 4C; Supplemental File 3). Representative example of hits
482 belonging to each phenotypic category are shown is Supplemental Fig. 1.

483 **Modulation of NOTCH1 localization and signaling by *PTPN23***

484 Considering the role of endocytosis in the regulation of Notch localization, to validate HCS
485 hits, we began from *PTPN23*, one of the 8 identified genes that have been previously associated
486 with regulation of endo-lysosomal trafficking (16% of the 51 hits: *CPA2, CTSE, MLC1, PIK3C2G,*
487 *PTPN23, TINAGL1, ZNRF1, ZNRF2*). *PTPN23* encodes HD-PTP, a ubiquitous nonreceptor
488 tyrosine pseudophosphatase that has been involved extensively in endosomal sorting,
489 multivesicular body formation (MVB) and ESCRT activity [50,51]. Automated analysis of HCS IF
490 images revealed that relative to control cells in which NOTCH1 mainly resided at the PM, *PTPN23*
491 KD MCF10A cells exhibited marked intracellular NOTCH1 accumulation, which appeared as
492 puncta (Supplemental Fig. 2A). We reasoned that *PTPN23* depletion might interfere with
493 NOTCH1 endosomal trafficking or sorting. To identify the compartment in which the NOTCH1

494 accumulated, we co-stained cells with antibodies against NOTCH1 and the endo-lysosomal
495 markers EEA1 or LAMP1, which identify early endosomes and lysosomes, respectively. Efficient
496 depletion of *PTPN23* (Supplemental Fig. 2B) led to significant expansion of the cytoplasmic pool
497 of puncta positive for EEA1, LAMP1, and NOTCH1 (Fig. 5A, quantified in A'). Quantitative
498 analysis also revealed that the NOTCH1 that accumulated upon *PTPN23* depletion mainly resided
499 in puncta positive for EEA1 (Fig. 5A'). Taken together, these data indicated that *PTPN23* depletion
500 might interfere with early to late endosomal trafficking, thereby trapping NOTCH1 mostly in early
501 endosomes.

502 We next evaluated how loss of *PTPN23* might affect Notch processing and signaling.
503 Western blot analysis revealed a marked reduction of both N1FL and N1TM upon *PTPN23* KD
504 (Fig. 5B) but surprisingly, the levels of N1ICD were not significantly altered, both in unstimulated
505 and stimulated conditions (Fig. 5C). To assess the effect of *PTPN23* depletion on Notch signaling,
506 we measured Notch-mediated RBPj-luc expression and found that when compared with control
507 cells, *PTPN23* silencing significantly suppressed Notch signaling in unstimulated conditions but
508 not in the presence of EGTA (Fig. 5D). Similar observations were obtained when measuring *HES1*
509 expression by quantitative reverse transcription PCR (RT-qPCR) (Fig 5E). Because reduced
510 biosynthetic N1FL levels could also result from low *NOTCH1* transcription, we also measured
511 *NOTCH1* mRNA levels and found that upon *PTPN23* depletion, *NOTCH1* expression levels were
512 mildly but significantly reduced (Fig 5F). These data indicate that *PTPN23* is required for NOTCH1
513 sorting into MVBs and for sustaining Notch expression and basal signaling and illustrate the
514 screen's ability to identify novel modulators of NOTCH1 trafficking and signaling.

515 **HCN2 silencing traps NOTCH1 in an enlarged GA and suppresses Notch signaling**

516 Automated analysis of HCS IF images identified 4 genes encoding channels (*CACNB4,*
517 *TRPM7, HCN2*, and *MLC1*) that upon KD in unstimulated conditions, caused cytosolic NOTCH1
518 accumulation (out of a total of 44 hits, a 9.1% enrichment; Supplemental file 3). Of these, *HCN2*

519 KD led to the most striking phenotype, with strong NOTCH1 accumulation in the perinuclear space
520 when compared with mock-silenced (non-targeting/NT) controls (Supplemental Fig. 3A). To test
521 if NOTCH1 accumulated in the perinuclear GA, we knocked down *HCN2* (Supplemental Fig. 3B)
522 and co-stained for NOTCH1 and the GA protein GIANTIN. Confocal analysis confirmed the
523 perinuclear NOTCH1 localization observed in the HCS images and revealed an expansion of the
524 Giantin-positive GA and increased localization of NOTCH1 in such compartment, when compared
525 to control cells (Fig. 6A, quantified in A'). Additionally, the analysis revealed that when compared
526 with the control, *HCN2* silencing markedly reduced cell surface NOTCH1 levels (Fig 6A, quantified
527 in A'), suggesting that HCN2 silencing might interfere with trafficking of newly made NOTCH1 to
528 the cell surface. To assess this, we compared NOTCH1 and EGFR localization upon *HCN2* KD
529 and 4-hour EGTA treatment. Both NOTCH1 and EGFR mostly failed to return to the PM after 1
530 or 4-hour w/o (Supplemental Fig. 4A; quantified in A'), indicating that both receptors do not traffic
531 efficiently to the PM in the absence of HCN2. Relative to mock silencing, *HCN2* depletion also led
532 to alteration of the TGN with loss of TGN46 and slight elevation of Golgin-97 (Fig 6B, quantified
533 in B').

534 Next, we extended the analysis of *HCN2* KD to Notch signaling output. *HCN2* depletion
535 significantly reduced expression of a Notch signaling reporter in unstimulated cells and limited the
536 expression of the NOTCH1 target gene, *HES1*, relative to controls (Fig. 6C–D). Consistent with
537 these observations, Western blot analysis revealed that when compared with the control, *HCN2*
538 silencing markedly reduced the levels of N1ICD both in the absence and presence of EGTA (Fig.
539 6E). Intriguingly, Western blot analysis of the levels of the S1 substrate, N1FL, revealed the
540 opposite trend, with *HCN2* KD elevating N1FL levels relative to the control (Fig. 6F; Supplemental
541 Fig. 3D). In contrast, the levels of N1TM, the S2-processed form of NOTCH1, were reduced in
542 *HCN2* KD cells, when compared with controls (Fig. 6F). Together, these findings suggest that
543 HCN2 is required to support a TGN organization that allows NOTCH1 S1 processing, PM delivery
544 and signaling.

545 **SGK3 silencing elevates cytosolic NOTCH1 levels**

546 Automated image analysis identified 5 kinases that when silenced, interfered with
547 NOTCH1 localization (*DCK, EIF2AK1, MASTL, PIK3C2G, SGK3* (corresponding to 9.8% of 51
548 hits; Supplemental File 3). Of these, *SGK3* might regulate Notch receptor stability based on
549 previous findings that SGK3 targets NDRG1 for FBW7-mediated proteasomal degradation [52],
550 a process that also limits N1ICD stability [53]. Moreover, the SGK3 paralog, SGK1, has previously
551 been reported to negatively modulate Notch signaling by targeting NOTCH1 for proteasomal
552 degradation [54]. Automated HCS image analysis revealed that relative to mock silencing,
553 efficient *SGK3* KD causes marked NOTCH1 accumulation in the cytosol (Supplemental Fig. 5).
554 To validate this observation, we silenced *SGK3* and analyzed the cells by confocal microscopy
555 after co-staining with antibodies against GOLGIN-97, EEA1 and LAMP1, to mark the early TGN,
556 early endosomes, and lysosomes, respectively. This analysis confirmed the presence of elevated
557 intracellular NOTCH1 levels but revealed no significant difference in its colocalization with the
558 Golgin-97-, EEA1- and LAMP1-positive compartments (Fig. 7A-B, quantified in A'-B'). We also
559 observed a significant elevation of EEA1 and LAMP1 puncta, suggesting that SGK3 might
560 regulate the endocytic compartment.

561 Given the diffused accumulation of NOTCH1 observed upon *SGK3* silencing, we
562 wondered whether this correlated with elevated NOTCH1 processing and signaling levels. We
563 first tested which NOTCH1 form accumulated upon *SGK3* KD and found that *SGK3* depletion
564 leads to elevated N1FL, N1TM, and N1ICD levels in both unstimulated and stimulated conditions
565 (Fig. 7C–D). We next used the Notch signaling reporter cell line MCF10A-RbpJk-Luc and
566 observed that when compared with the control, silencing *SGK3* caused significantly higher Notch
567 signaling output upon EGTA stimulation (Fig. 7E). Although signaling did not differ significantly in
568 unstimulated *SGK3*-silenced MCF10A-RbpJk-Luc cells when compared to mock silencing, RT-
569 qPCR analysis revealed that *SGK3* KD in MCF10A cells significantly upregulated the expression

570 of the Notch signaling targets *HEY1,* but not HES1. Depletion lead also to a slight transcriptional
571 elevation of NOTCH1 (Fig. 7F–H).

572 The observation that depleting *SGK3* in MCF10A cells leads to elevated N1ICD levels
573 made us wonder whether SGK3 reduction might impair N1ICD degradation. To test this
574 possibility, we silenced *SGK3* and then treated the cells with cycloheximide (CHX) to block protein
575 synthesis or with DMSO as a negative control. Because blocking the synthesis of new proteins
576 would allow cells to turn over proteins that had been present before CHX addition, we reasoned
577 that if SGK3 is required for efficient N1ICD degradation, upon CHX treatment *SGK3*-depleted
578 cells would exhibit elevated N1ICD levels when compared with control cells. Western blot analysis
579 using antibodies against N1FL and N1ICD revealed that *SGK3* silencing caused marked increase
580 in the levels of N1FL and N1ICD when compared with control. However, N1FL and N1ICD levels
581 were markedly decreased in both control and *SGK3* KD cells upon CHX treatment (Fig. 7I),
582 indicating that SGK3 is not required for N1ICD destabilization. Finally, to assess whether SGK3
583 contributed directly or indirectly to N1ICD phosphorylation, we silenced *SGK3* in MCF10A cells
584 and then performed the λ-PPA assay. This analysis revealed that in *SGK3* KD cells, accumulated
585 N1ICD was still phosphorylated, and that phosphorylation could be erased by treating the cell
586 extracts with λ-PPA (Fig. 7J), indicating that SGK3 is not required for N1ICD phosphorylation.
587 Taken together, these data indicate that SGK3 negatively regulates NOTCH1 levels and signaling
588 indirectly by a mechanism other than control of N1ICD stability and/or degradation.

589 **Pharmacologic SGK3 inhibition elevates N1ICD levels and Notch signaling**

590 To explore whether SGK3 modulation of NOTCH1 could be controlled pharmacologically,
591 we examined the effect of VPS34-IN1, a well characterized SGK3 inhibitor [55,56]. We first tested
592 if VPS34-IN1 can effectively block SGK3 activity in MCF10A cells. Because we were unable to
593 directly evaluate SGK3 phosphorylation upon treatment of cultured cells with VPS34-IN1, we
594 evaluated the phosphorylation levels of NDRG1, a known SGK3 substrate [52,57]. SGK3 can be

595 activated by stimulating the cells with growth factors, such as IGF1 and EGF [58–60]. Thus, we
596 stimulated control or VPS34-IN1-treated cells with EGF to promote NDRG1 phosphorylation.
597 Strikingly, EGF failed to elicit NDRG1 phosphorylation in VPS34-IN1-treated cells and erased the
598 basal low level of NDRG1 phosphorylation in unstimulated cells (Fig 8A), indicating that treatment
599 with VPS34-IN1 potently blocks SGK3 activity in cultured MCF10A cells.

600 Next, to determine if pharmacologic VPS34-IN1 treatment reproduces the effects of *SGK3*
601 silencing on NOTCH1, we treated MCF10A cells with VPS34-IN1 and measured N1ICD levels.
602 Western blot analysis revealed that relative to mock treatment, VPS34-IN1 significantly elevated
603 the levels of N1ICD (Fig 8B). To establish whether VPS34-IN1 treatment also elevates Notch
604 targets, we examined the expression levels of *HEY1* by RT-qPCR. This analysis revealed that
605 when compared with control cells, *HEY1* levels were significantly higher in VPS34-IN1-treated
606 cells (Fig. 8C). Taken together, these data indicate that as with *SGK3* silencing, pharmacologic
607 VPS34-IN1 treatment elevates NOTCH1 levels and promotes Notch signaling.

608 **A secondary screen using a Notch reporter identifies 39 new modulators of NOTCH1**
609 **localization that affect signaling output**

610 To systematically determine the impact of the modulators of NOTCH1 trafficking on Notch
611 signaling, we individually silenced with esiRNA the 231 primary hits in MCF10A-RbpJk-Luc cells
612 with or without EGTA stimulation and measured signaling output. We included *PTPN23* and *SGK3*
613 as positive controls since their positive contribution to unstimulated signaling and negative
614 contribution to stimulated signaling had been assessed during the validation of the NOTCH1
615 localization screen. As expected, *PTPN23* and *SGK3* depletion reproduced previous evidence.
616 Focusing on the validated 51 genes that affect localization in the secondary screen, the analysis
617 identified 39 depletions (76.5% of the total) that altered Notch signaling by at least 30%, with 21
618 modulating signaling in unstimulated conditions only, 8 in stimulated conditions only, and 10 in
619 both conditions (Fig. 9A–C; Supplemental File 3). Of the 39 depletions, 30 led to reduced signaling

620 (9 of which also in stimulated conditions), while 9 led to increased signaling (8 of which in
621 stimulated conditions (Fig 9D). The NOTCH1 localization phenotypic classes of the 39 depletions
622 are reported in Fig. 9D, while information about signaling modulation by the set of 231 siRNA of
623 the primary screen is included in Supplemental File 2. This approach led to the identification of
624 several new positive and negative regulators of Notch signaling that require further
625 characterization.

626 **Discussion**

627 NOTCH1 activity in MCF10A cells has been mostly characterized using transfection of
628 activated forms [61,62]. Here, we have shown that in MCF10A cells is possible to activate
629 endogenous NOTCH1 using a short pulse of Ca^{2+} chelation that destabilizes the NOTCH1 HD
630 domain leading to S2 and S3 cleavage, as previously reported for a variety of different cell types
631 [6,63–65]. Interestingly, we find that confluent MCF10A cells possess a low level basal S3
632 cleavage and that, upon S3 cleavage NOTCH1 is rapidly phosphorylated, an event that has been
633 described to lead to proteasomal degradation of NICD. Whether such basal S3 cleavage depends
634 on transactivation among neighboring cells, considering that MCF10A cells also express
635 NOTCH1 ligands [34], or whether it is a cell autonomous occurrence due to intracellular ligand-
636 independent activation remains to be determined.

637 By means that inhibit lysosomal degradation, we also have determined that trafficking of
638 endogenous NOTCH1 in MCF10A cells occurs similarly to what has been reported *in vivo* in
639 epithelial imaginal discs of *Drosophila melanogaster* [66]. Interestingly, upon inhibition of
640 lysosomal degradation, endogenous NOTCH1 and EGFR not only accumulate in lysosomes but
641 are also depleted from the PM, suggesting that some coordination of new synthesis and/or ER to
642 PM trafficking with clearance might exist. Transit kinetics indicate that NOTCH1 traffics from the
643 ER to the GA in less than 1 hour and from the GA to PM in as little as 3 hours. These times
644 suggest that on average the half-life of each NOTCH1 molecule is only approximately 4 hours, a

645 time comparable to previous *in vivo* findings using *Drosophila* Notch [67]. Such half-life is also
646 compatible with the two main events described during NOTCH1 secretion, namely receptor
647 glycosylation and S1 cleavage by Furin [68,69].

648 Because the half-life of NOTCH1 is very limited, we posited that genetic perturbations
649 could result in visible changes in NOTCH1 localization. Such possibility suggested that high
650 throughput determination of steady-state NOTCH1 localization could uncover new genes that are
651 important for NOTCH1 localization and associated events of activation, as well as new genes that
652 regulate trafficking or compartment organization in MCF10A cells. We identified 51 putative genes
653 that alter NOTCH1 localization of which 39 resulted in modulation of signaling. We validated hits
654 with an alternative set of reagents to exclude the possibility of off target or nonspecific effects.
655 Most of the identified genes are expressed in MCF10A cells according to recent RNAseq analyses
656 [70,71]. While some of the candidate genes, especially those obtained upon EGTA stimulation,
657 might be the result of indirect or combined effects with the transient extracellular Ca^{2+} depletion
658 used to activate signaling, 31, the vast majority, have been identified in unstimulated conditions,
659 indicating that tight NOTCH1 trafficking regulation is crucial for determining basal levels of
660 signaling. Interestingly, among these 31 basal signaling genes, 30 are required to promote RbpJk
661 transcriptional activity, while only *CALM2* appeared to negatively regulate signaling. These data
662 suggest that sustaining high Notch turnover enables basal signaling. Also, all 3 genes that we
663 have best characterized alter the distribution of markers of trafficking compartments, indicating
664 that the effect on NOTCH1 trafficking and signaling of the identified candidate genes is likely to
665 be indirect and mediated be supporting correct organization of trafficking compartments.

666 Several phenotype-based genome-wide Notch screens have been performed *in vivo*, in
667 animal models such as *Drosophila* [72–75] and in cellular systems [76,77]. Strikingly, paralogs of
668 12 genes out of the 51 that we have identified have been previously identified as modulators of
669 Notch phenotypes in previous screens (*CACNB4, CALM2, CIB2, CMPK1*, *CTSE, MAP3K12,*

670 *PIK3K2CG, PTPN23, TRPM7, USP36, UFD1L, ZNRF1*), suggesting that some of the candidates
671 might play a conserved function and might be validated in *in vivo* models.

672 Among genes that we have identified, some have previously been associated with
673 regulation of the mTOR pathway (*CIB2, MASTL, MC1R, SGK3, ZNRF1, ZNRF2*). ZNRF1 appears
674 to be required for EGFR sorting to late endosomes, a prerequisite for lysosomal degradation and
675 signaling termination [78]. In contrast, ZNRF2 has been found to regulate mTOR signaling at
676 lysosomes [79]. Also, the calcium and integrin binding protein 2 encoded by the gene *CIB2*, which
677 we found here as a negative regulator of NOTCH1, is a negative regulator of mTOR signaling in
678 the mouse retinal pigmented epithelium [80]. Similarly, the MASTL kinase regulates mTOR [81]
679 and EGFR [82]. Finally, as a NOTCH1 modulator we have found MC1R (Melacortin 1 receptor),
680 which in melanocytes contributes to pigmentation by regulating the TFEB paralog MITF, among
681 other pathways. Interestingly, agonists of MC1R are reported to modulate Notch signaling in
682 synovial fibroblast in models of arthritis [83], suggesting that coregulation of Notch and the
683 MC1R/MITF pathway might exist.

684 We have characterized the activity of *SGK3* as a negative regulator of NOTCH1
685 expression and signaling. *SGK3* encodes a PI3K-dependent endosome-localized
686 serine/threonine kinase with similar substrate specificity to AKT, a kinase acting upstream of
687 mTOR widely involved in tumorigenesis [83]. All forms of NOTCH1 accumulate in *SGK3* depleted
688 cells and we have excluded that SGK3 directly phosphorylates N1ICD. Thus, SGK3 is likely to
689 act indirectly on NOTCH1. Because SGK3 has been proposed to promote mTOR activation in
690 endo-lysosomal compartments, an interesting possibility is that mTOR and NOTCH1 might be
691 alternatively regulated. Interestingly, resistance to mTOR inhibition in breast cancer cells is
692 mediated by hVPS34 and SGK3, defining an AKT independent mTOR activation pathway [84].
693 Considering that inhibition of Notch activity on TNBCC abrogates *SGK3* expression [85], a
694 Notch/SGK3 regulatory loop might exist in breast cells, that will be further investigated in future.

695 Finally, it will be important to test whether SGK3 acts as a negative regulator in contexts in which
696 NOTCH1 acts as a tumor suppressor, such as during skin tumorigenesis [86].

697 The relocalization of NOTCH1 to early endosomes upon *PTPN23* KD matches earlier
698 observations in human cells that indicate that PTPN23 resides on early endosomes and that its
699 depletion causes EGFR accumulation in EEA1-positive endosomes [87]. The activity of PTPN23
700 on endocytic trafficking and ESCRT function is well documented [50,88,89]. However, we find
701 that NOTCH1 signaling activity upon *PTPN23* KD is slightly reduced, yet the loss of ESCRT
702 components usually enhances Notch signaling [31,33,66,90]. Considering that *PTPN23* has been
703 described as a tumor suppressor as is the case of ESCRT genes, and that loss of PTPN23
704 contributes to mammary tumorigenesis by altering endocytic trafficking of cancer-relevant
705 cargoes [91,92], it will be important in the future to understand whether Notch alteration
706 contributes to tumorigenesis initiated by loss of *PTPN23* in contexts in which Notch acts as a
707 tumor suppressor, as well as to further dissect the mechanistic relationship between Notch and
708 PTPN23.

709 In addition to *PTPN23* and *SGK3,* five other identified genes have been associated with
710 breast tumorigenesis (*GPCR, GPR125, MET, NUDT5, TINAGL1*). In fact, the gastrin-releasing
711 peptide receptor, a G protein couple receptor (GPCR) encoded by *GRPR* is an established marker
712 of prostate and breast cancers [93,94]. Loss of *TINAGL1* encoding the tubulointerstitial nephritis
713 antigen-like 1, a secreted basement membrane inactive peptidase, has been identified as a
714 marker of poor breast cancer prognosis [95] and appears to negatively regulate Integrin and
715 EGFR signaling in triple negative breast cancer [96]. In addition, the NUDIX hydrolase type 5
716 encoded by *NUDT5* is an ADP-ribose pyrophosphatase and nucleotide metabolizing enzyme
717 involved in regulation of AKT in breast cancer [97]. It generates nuclear ATP to fuel chromatin
718 remodeling, gene expression, and proliferation [98]. Also, *GPR125* encodes a GPCR that
719 regulates epithelial polarity [99] and is associated with poor outcome in breast cancer [100].
720 Finally, *MET,* which encodes the hepatocyte growth factor receptor (HGFR), is a proto-oncogenic

721 receptor tyrosine kinase found to be coregulated with Notch in physiologic as well as several
722 pathologic conditions, including in gastric and breast cancer cells [101–105]. These combined
723 studies warrant further characterization of the identified candidate genes in breast cancer cells.

724 A few genes that we have isolated in the screen have been previously involved in
725 regulation of Notch signaling (*ADORA1, CALM2, JAK3, MAP3K12, PLAU, TRPM7*). Inhibition of
726 adenosine A1 receptor encoded by *ADORA1* has been recently implicated in Notch dependent
727 signaling in lung cancer cells [106]. Also, Notch signaling activation triggers JAK3 ubiquitination
728 and degradation [107]. In addition, NOTCH1 activates *PLAU* encoding the urokinase-type
729 plasminogen activator, a secreted ECM enzyme, in migrating mouse keratinocytes [108].

730 Some of the identified genes that have previously been associated with Notch signaling
731 appear connected with cation regulation, even if we identified the vast majority in unstimulated
732 conditions (*CALM2, HCN2, MAP3K12, TRPM7*). A case in point is that of *TRPM7,* encoding the
733 transient receptor potential melastatin-related 7, a divalent Ca^{2+} and Mg^{2+} channel fused with a
734 functional serine/threonine-protein kinase that is widely overexpressed in breast cancer (reviewed
735 by [109]. Remarkably, *TRPM7* has been described as a potent inducer of Notch activation during
736 glial tumorigenesis [110,111]. Intriguingly, Mg^{2+} supplementation during osteogenesis appears to
737 activate NOTCH1 signaling, a phenomenon reverted by TRPM7 inhibition [112]. In addition, the
738 *Caenorhabditis elegans* homolog of MAP3K12 (also called DLK), a Ca^{2+} activated MAP kinase
739 involved in trafficking and signaling regulation that we identified [113,114], has been shown to
740 repress Notch signaling by activating autophagy in neurons [115]. Finally, the calmodulin-
741 encoding *CALM2* and CaMKIV activity have been reported to enhance NOTCH1 activity in
742 osteoclasts and prostate cancer cells [116,117], while calmodulin-dependent serine protein
743 kinase (CASK) does that in pancreatic cancer cells [118], and cardiovascular development [119].
744 This evidence suggests that changes in intracellular cation regulation might fine tune extracellular
745 and/or cytoplasmic Notch activation.

746 Our observation that expression of *HCN2* encoding the hyperpolarization-activated cyclic
747 nucleotide-gated channel 2 in MCF10A is required to support post-GA trafficking of NOTCH1 as
748 well as its S1 cleavage suggest that inhibition of HCN2 might reduce the oncogenic effects of
749 NOTCH1 when mutations do not liberate it from membranes. We observed a major alteration of
750 TGN morphology upon *HCN2* depletion in MCF10A cells. This suggest that GA trafficking to the
751 TGN might be supported by HCN2, thus leading to correct Furin cleavage of NOTCH1.
752 Importantly, recent data indicate that HCN2 is expressed in MCF10A cells and that it is
753 overexpressed in triple negative breast cancer cells. In the latter, inhibition or depletion of HCN2
754 leads to misregulation of intracellular Ca^{2+} regulation and ER stress [120]. This evidence suggests
755 that analysis of HCN2 inactivation in breast cancer, in particular the triple negative type that is
756 defined by elevated Notch activity (reviewed in [121]), could be beneficial.

757 In addition to these genes, we also identified as modifiers two genes that encode the
758 deubiquitinating enzymes (DUBs) USP36 and USP39. Silencing both leads to intracellular
759 accumulation of NOTCH1. However, *USP36* appears to promote signaling, while *USP39*
760 represses it. USP39, which does not possess deubiquitinating activity and is present in the
761 nucleus as a splicing factor [122,123], has been found to be in complex with the γ-secretase
762 component, Nicastrin, in large-scale proteomics of human cells [124]. USP36 is nucleolar and is
763 involved in ribosome biogenesis [125,126]. In contrast, in flies, USP36 represses autophagy [127]
764 and has been shown to control H2B ubiquitination and chromatin regulation leading to repression
765 of Notch signaling [128]. This evidence suggest that these DUBs could be involved in a conserved
766 network of Notch signaling regulation occurring in the nucleus.

767 Overall, the genes isolated in our screen expand the repertoire of factors regulating
768 intracellular trafficking and NOTCH1 localization and signaling. They also represent potential new
769 drug targets that may be relevant to breast tumorigenesis and other Notch-associated
770 pathologies.

771

772 **References**

773 1. Artavanis-Tsakonas S, Rand MD, Lake RJ, Artavanis-Tsakonas S, Rand MD, Lake RJ. Notch
774 signaling: cell fate control and signal integration in development. Science. 1999;284: 770–776.
775 doi:10.1126/science.284.5415.770

776 2. Andersson ER, Sandberg R, Lendahl U. Notch signaling: simplicity in design, versatility in function.
777 Development. 2011;138: 3593–612. doi:10.1242/dev.063610

778 3. Koch U, Lehal R, Radtke F. Stem cells living with a Notch. Development. 2013;140: 689–704.
779 doi:10.1242/dev.080614

780 4. Mašek J, Andersson ER. The developmental biology of genetic Notch disorders. Development.
781 2017;144: 1743–1763. doi:10.1242/DEV.148007

782 5. Blaumueller CM, Qi H, Zagouras P, Artavanis-Tsakonas S. Intracellular Cleavage of Notch Leads to
783 a Heterodimeric Receptor on the Plasma Membrane. Cell. 1997;90: 281–291. doi:10.1016/S0092-
784 8674(00)80336-0

785 6. Rand MD, Grimm LM, Artavanis-Tsakonas S, Patriub V, Blacklow SC, Sklar J, et al. Calcium
786 depletion dissociates and activates heterodimeric notch receptors. Mol Cell Biol. 2000;20: 1825–
787 35. Available: http://www.ncbi.nlm.nih.gov/pubmed/10669757

788 7. Kopan R, Ilagan MXG. The Canonical Notch Signaling Pathway: Unfolding the Activation
789 Mechanism. Cell. 2009;137: 216–233. doi:10.1016/j.cell.2009.03.045

790 8. van Tetering G, van Diest P, Verlaan I, van der Wall E, Kopan R, Vooijs M. Metalloprotease
791 ADAM10 is required for NOTCH1 site 2 cleavage. Journal of Biological Chemistry. 2009;284:
792 31018–31027. doi:10.1074/jbc.M109.006775

793 9. Herreman A, Serneels L, Annaert W, Collen D, Schoonjans L, de Strooper B. Total inactivation of
794 gamma-secretase activity in presenilin-deficient embryonic stem cells. Nat Cell Biol. 2000;2: 461–
795 2. doi:10.1038/35017105

796 10. Schroeter EH, Kisslinger JA, Kopan R. Notch-1 signalling requires ligand-induced proteolytic
797 release of intracellular domain. Nature. 1998;393: 382–6. doi:10.1038/30756

798 11. Zhang Z, Nadeau P, Song W, Donoviel D, Yuan M, Bernstein A, et al. Presenilins are required for
799 gamma-secretase cleavage of beta-APP and transmembrane cleavage of Notch-1. Nat Cell Biol.
800 2000;2: 463–5. doi:10.1038/35017108

801 12. Bray SJ. Notch signalling: a simple pathway becomes complex. Nat Rev Mol Cell Biol. 2006;7:
802 678–89. doi:10.1038/nrm2009

803 13. Tagami S, Okochi M, Yanagida K, Ikuta A, Fukumori A, Matsumoto N, et al. Regulation of Notch
804 signaling by dynamic changes in the precision of S3 cleavage of Notch-1. Mol Cell Biol. 2008;28:
805 165–76. doi:10.1128/MCB.00863-07

806 14. Hori K, Sen A, Kirchhausen T, Artavanis-Tsakonas S. Regulation of ligand-independent Notch
807 signal through intracellular trafficking. Commun Integr Biol. 2012;5: 374–6.
808 doi:10.4161/cib.19995

809 15. Fortini ME, Bilder D. Endocytic regulation of Notch signaling. Curr Opin Genet Dev. 2009;19: 323–
810 8. doi:10.1016/j.gde.2009.04.005

811 16. Moretti J, Brou C. Ubiquitinations in the notch signaling pathway. Int J Mol Sci. 2013;14: 6359–81.
812 doi:10.3390/ijms14036359

813 17. Sakata T, Sakaguchi H, Tsuda L, Higashitani A, Aigaki T, Matsuno K, et al. Drosophila Nedd4
814 regulates endocytosis of notch and suppresses its ligand-independent activation. Curr Biol.
815 2004;14: 2228–36. doi:10.1016/j.cub.2004.12.028

816 18. Schneider M, Troost T, Grawe F, Martinez-Arias A, Klein T. Activation of Notch in lgd mutant cells
817 requires the fusion of late endosomes with the lysosome. J Cell Sci. 2013;126: 645–56.
818 doi:10.1242/jcs.116590

819 19. Panin VM, Papayannopoulos V, Wilson R, Irvine KD. Fringe modulates Notch-ligand interactions.
820 Nature. 1997;387: 908–912. doi:10.1038/43191

821 20. Acar M, Jafar-Nejad H, Takeuchi H, Rajan A, Ibrani D, Rana NA, et al. Rumi is a CAP10 domain
822 glycosyltransferase that modifies Notch and is required for Notch signaling. Cell. 2008;132: 247–
823 258. doi:10.1016/J.CELL.2007.12.016

824 21. Shi S, Stanley P. Protein O-fucosyltransferase 1 is an essential component of Notch signaling
825 pathways. Proc Natl Acad Sci U S A. 2003;100: 5234–5239. doi:10.1073/PNAS.0831126100

826 22. Seugnet L, Simpson P, Haenlin M. Requirement for dynamin during Notch signaling in Drosophila
827 neurogenesis. Dev Biol. 1997;192: 585–598. doi:10.1006/dbio.1997.8723

828 23. Xu T, Artavanis-Tsakonas S. deltex, a locus interacting with the neurogenic genes, Notch, Delta
829 and mastermind in Drosophila melanogaster. Genetics. 1990;126: 665–77. Available:
830 http://www.pubmedcentral.nih.gov/articlerender.fcgi?artid=1204222&tool=pmcentrez&rendert
831 ype=abstract

832 24. Matsuno K, Diederich RJ, Go MJ, Blaumueller CM, Artavanis-Tsakonas S. Deltex acts as a positive
833 regulator of Notch signaling through interactions with the Notch ankyrin repeats. Development.
834 1995;121: 2633–44. Available: http://www.ncbi.nlm.nih.gov/pubmed/7671825

835 25. Diederich RJ, Matsuno K, Hing H, Artavanis-Tsakonas S. Cytosolic interaction between deltex and
836 Notch ankyrin repeats implicates deltex in the Notch signaling pathway. Development. 1994;120:
837 473–81. Available: http://www.ncbi.nlm.nih.gov/pubmed/8162848

838 26. Kishi N, Tang Z, Maeda Y, Hirai A, Mo R, Ito M, et al. Murine homologs of deltex define a novel
839 gene family involved in vertebrate Notch signaling and neurogenesis. International Journal of
840 Developmental Neuroscience. 2001;19: 21–35. doi:10.1016/S0736-5748(00)00071-X

841 27. Hori K, Fostier M, Ito M, Fuwa TJ, Go MJ, Okano H, et al. Drosophila deltex mediates suppressor
842 of Hairless-independent and late-endosomal activation of Notch signaling. Development.
843 2004;131: 5527–37. doi:10.1242/dev.01448

844 28. Cornell M, Evans DA, Mann R, Fostier M, Flasza M, Monthatong M, et al. The Drosophila
845 melanogaster Suppressor of deltex gene, a regulator of the Notch receptor signaling pathway, is
846 an E3 class ubiquitin ligase. Genetics. 1999;152: 567–76. Available:
847 http://www.pubmedcentral.nih.gov/articlerender.fcgi?artid=1460625&tool=pmcentrez&rendert
848 ype=abstract

849 29. Chastagner P, Israël A, Brou C, Chastagner P, Israe A, Israël A, et al. AIP4/Itch regulates Notch
850 receptor degradation in the absence of ligand. Wölfl S, editor. PLoS One. 2008;3: e2735.
851 doi:10.1371/journal.pone.0002735

852 30. Wilkin MB, Carbery A-M, Fostier M, Aslam H, Mazaleyrat SL, Higgs J, et al. Regulation of Notch
853 Endosomal Sorting and Signaling by Drosophila Nedd4 Family Proteins. Current Biology. 2004;14:
854 2237–2244. doi:10.1016/j.cub.2004.11.030

855 31. Vaccari T, Bilder D. The Drosophila tumor suppressor vps25 prevents nonautonomous
856 overproliferation by regulating notch trafficking. Dev Cell. 2005;9: 687–98.
857 doi:10.1016/j.devcel.2005.09.019

858 32. Hori K, Sen A, Kirchhausen T, Artavanis-Tsakonas S. Synergy between the ESCRT-III complex and
859 Deltex defines a ligand-independent Notch signal. J Cell Biol. 2011;195: 1005–15.
860 doi:10.1083/jcb.201104146

861 33. Thompson BJ, Mathieu J, Sung H-H, Loeser E, Rørth P, Cohen SM. Tumor suppressor properties of
862 the ESCRT-II complex component Vps25 in Drosophila. Dev Cell. 2005;9: 711–20.
863 doi:10.1016/j.devcel.2005.09.020

864 34. Kobia F, Duchi S, Deflorian G, Vaccari T. Pharmacologic inhibition of vacuolar H+ ATPase reduces
865 physiologic and oncogenic Notch signaling. Mol Oncol. 2014;8: 207–20.
866 doi:10.1016/j.molonc.2013.11.002

867 35. Kozik P, Hodson N a, Sahlender DA, Simecek N, Soromani C, Wu J, et al. A human genome-wide
868 screen for regulators of clathrin-coated vesicle formation reveals an unexpected role for the V-
869 ATPase. Nat Cell Biol. 2013;15: 50–60. doi:10.1038/ncb2652

870 36. Yan Y, Denef N, Schüpbach T, Schu T, Schüpbach T. The Vacuolar Proton Pump, V-ATPase, Is
871 Required for Notch Signaling and Endosomal Trafficking in Drosophila. Dev Cell. 2009;17: 387–
872 402. doi:10.1016/j.devcel.2009.07.001

873 37. Lange C, Prenninger S, Knuckles P, Taylor V, Levin M, Calegari F. The H(+) vacuolar ATPase
874 maintains neural stem cells in the developing mouse cortex. Stem Cells Dev. 2011;20: 843–50.
875 doi:10.1089/scd.2010.0484

876 38. Sethi N, Yan Y, Quek D, Schupbach T, Kang Y. Rabconnectin-3 is a functional regulator of
877 mammalian notch signaling. Journal of Biological Chemistry. 2010;285: 34757–34764.
878 doi:10.1074/jbc.M110.158634

879 39. Vaccari T, Duchi S, Cortese K, Tacchetti C, Bilder D. The vacuolar ATPase is required for
880 physiological as well as pathological activation of the Notch receptor. Development. 2010;137:
881 1825–1832. doi:10.1242/dev.045484

882 40. Valapala M, Hose S, Gongora C, Dong L, Wawrousek EF, Samuel Zigler J, et al. Impaired
883 endolysosomal function disrupts Notch signalling in optic nerve astrocytes. Nat Commun. 2013;4:
884 1629. doi:10.1038/ncomms2624

885 41. Birmingham A, Selfors LM, Forster T, Wrobel D, Kennedy CJ, Shanks E, et al. Statistical methods
886 for analysis of high-throughput RNA interference screens. Nat Methods. 2009;6: 569–75.
887 doi:10.1038/nmeth.1351

888 42. Soule HD, Maloney TM, Wolman SR, Peterson WD, Brenz R, McGrath CM, et al. Isolation and
889 characterization of a spontaneously immortalized human breast epithelial cell line, MCF-10.
890 Cancer Res. 1990;50: 6075–86. Available: http://www.ncbi.nlm.nih.gov/pubmed/1975513

891 43. Fryer CJ, White JB, Jones KA. Mastermind recruits CycC:CDK8 to phosphorylate the Notch ICD and
892 coordinate activation with turnover. Mol Cell. 2004;16: 509–520.
893 doi:10.1016/j.molcel.2004.10.014

894 44. Morrugares R, Correa-Sáez A, Moreno R, Garrido-Rodríguez M, Muñoz E, de la Vega L, et al.
895 Phosphorylation-dependent regulation of the NOTCH1 intracellular domain by dual-specificity
896 tyrosine-regulated kinase 2. Cellular and Molecular Life Sciences. 2020;77: 2621.
897 doi:10.1007/S00018-019-03309-9

898 45. Li N, Fassl A, Chick J, Inuzuka H, Li X, Mansour MR, et al. Cyclin C is a haploinsufficient tumor
899 suppressor. Nat Cell Biol. 2014;16: 1080. doi:10.1038/NCB3046

900 46. Satinover DL, Leach CA, Stukenberg PT, Brautigan DL. Activation of Aurora-A kinase by protein
901 phosphatase inhibitor-2, a bifunctional signaling protein. Proc Natl Acad Sci U S A. 2004;101:
902 8625. doi:10.1073/PNAS.0402966101

903 47. Hay JC. Calcium: A fundamental regulator of intracellular membrane fusion? EMBO Reports.
904 European Molecular Biology Organization; 2007. pp. 236–240. doi:10.1038/sj.embor.7400921

905 48. Pryor PR, Mullock BM, Bright NA, Gray SR, Luzio JP. The role of intraorganellar Ca2+ in late
906 endosome-lysosome heterotypic fusion and in the reformation of lysosomes from hybrid
907 organelles. Journal of Cell Biology. 2000;149: 1053–1062. doi:10.1083/jcb.149.5.1053

908 49. Theis M, Buchholz F. MISSION esiRNA for RNAi screening in mammalian cells. Journal of
909 Visualized Experiments. 2010 [cited 24 Mar 2021]. doi:10.3791/2008

910 50. Doyotte A, Mironov A, McKenzie E, Woodman P. The Bro1-related protein HD-PTP/PTPN23 is
911 required for endosomal cargo sorting and multivesicular body morphogenesis. Proc Natl Acad Sci
912 U S A. 2008;105: 6308. doi:10.1073/PNAS.0707601105

913 51. Tabernero L, Woodman P. Dissecting the role of His domain protein tyrosine
914 phosphatase/PTPN23 and ESCRTs in sorting activated epidermal growth factor receptor to the
915 multivesicular body. Biochemical Society Transactions. Portland Press Ltd; 2018. pp. 1037–1046.
916 doi:10.1042/BST20170443

917 52. Gasser JA, Inuzuka H, Lau AW, Wei W, Beroukhim R, Toker A. SGK3 Mediates INPP4B-Dependent
918 PI3K Signaling in Breast Cancer. Mol Cell. 2014;56: 595–607. doi:10.1016/j.molcel.2014.09.023

919 53. Oberg C, Li J, Pauley A, Wolf E, Gurney M, Lendahl U. The Notch Intracellular Domain Is
920 Ubiquitinated and Negatively Regulated by the Mammalian Sel-10 Homolog. Journal of Biological
921 Chemistry. 2001;276: 35847–35853. doi:10.1074/jbc.M103992200

922 54. Mo JS, Ann EJ, Yoon JH, Jung J, Choi YH, Kim HY, et al. Serum- and glucocorticoid-inducible kinase
923 1 (SGK1) controls notch1 signaling by downregulation of protein stability through Fbw7 ubiquitin
924 ligase. J Cell Sci. 2011;124: 100–112. doi:10.1242/jcs.073924

925 55. Bago R, Malik N, Munson MJ, Prescott AR, Davies P, Sommer E, et al. Characterization of VPS34-
926 IN1, a selective inhibitor of Vps34, reveals that the phosphatidylinositol 3-phosphate-binding
927 SGK3 protein kinase is a downstream target of class III phosphoinositide 3-kinase. Biochemical
928 Journal. 2014;463: 413–427. doi:10.1042/BJ20140889

929 56. Ronan B, Flamand O, Vescovi L, Dureuil C, Durand L, Fassy F, et al. A highly potent and selective
930 Vps34 inhibitor alters vesicle trafficking and autophagy. Nat Chem Biol. 2014;10: 1013–1019.
931 doi:10.1038/nchembio.1681

932 57. Tovell H, Testa A, Zhou H, Shpiro N, Crafter C, Ciulli A, et al. Design and Characterization of SGK3-
933 PROTAC1, an Isoform Specific SGK3 Kinase PROTAC Degrader. ACS Chem Biol. 2019;14: 2024–
934 2034. doi:10.1021/acschembio.9b00505

935 58. Kobayashi T, Deak M, Morrice N, Cohen P. Characterization of the structure and regulation of two
936 novel isoforms of serum- and glucocorticoid-induced protein kinase. Biochemical Journal.
937 1999;344: 189–197. doi:10.1042/0264-6021:3440189

938 59. Virbasius J v., Song X, Pomerleau DP, Zhan Y, Zhou GW, Czech MP. Activation of the Akt-related
939 cytokine-independent survival kinase requires interaction of its phox domain with endosomal
940 phosphatidylinositol 3-phosphate. Proc Natl Acad Sci U S A. 2001;98: 12908–12913.
941 doi:10.1073/pnas.221352898

942 60. Malik N, Macartney T, Hornberger A, Anderson KE, Tovell H, Prescott AR, et al. Mechanism of
943 activation of SGK3 by growth factors via the Class 1 and Class 3 PI3Ks. Biochemical Journal.
944 2018;475: 117–135. doi:10.1042/BCJ20170650

945 61. Mazzone M, Selfors LM, Albeck J, Overholtzer M, Sale S, Carroll DL, et al. Dose-dependent
946 induction of distinct phenotypic responses to Notch pathway activation in mammary epithelial
947 cells. Proc Natl Acad Sci U S A. 2010;107: 5012–5017. doi:10.1073/PNAS.1000896107

948 62. Meurette O, Stylianou S, Rock R, Collu GM, Gilmore AP, Brennan K. Notch activation induces Akt
949 signaling via an autocrine loop to prevent apoptosis in breast epithelial cells. Cancer Res.
950 2009;69: 5015–22. doi:10.1158/0008-5472.CAN-08-3478

951 63. Tremblay I, Paré E, Arsenault D, Douziech M, Boucher MJ. The MEK/ERK Pathway Promotes
952 NOTCH Signalling in Pancreatic Cancer Cells. PLoS One. 2013;8: 85502.
953 doi:10.1371/JOURNAL.PONE.0085502

954 64. Swaminathan B, Youn SW, Naiche LA, Du J, Villa SR, Metz JB, et al. Endothelial Notch signaling
955 directly regulates the small GTPase RND1 to facilitate Notch suppression of endothelial
956 migration. Scientific Reports 2022 12:1. 2022;12: 1–14. doi:10.1038/s41598-022-05666-1

957 65. Westhoff B, Colaluca IN, D'Ario G, Donzelli M, Tosoni D, Volorio S, et al. Alterations of the Notch
958 pathway in lung cancer. Proc Natl Acad Sci U S A. 2009;106: 22293–22298.
959 doi:10.1073/PNAS.0907781106/SUPPL_FILE/0907781106SI.PDF

960 66. Vaccari T, Lu H, Kanwar R, Fortini ME, Bilder D. Endosomal entry regulates Notch receptor
961 activation in Drosophila melanogaster. J Cell Biol. 2008;180: 755–62. doi:10.1083/jcb.200708127

962 67. Couturier L, Trylinski M, Mazouni K, Darnet L, Schweisguth F. A fluorescent tagging approach in
963 Drosophila reveals late endosomal trafficking of Notch and Sanpodo. J Cell Biol. 2014;207: 351.
964 doi:10.1083/JCB.201407071

965 68. Sasamura T, Ishikawa HO, Sasaki N, Higashi S, Kanal M, Nakao S, et al. The O-fucosyltransferase
966 O-fut1 is an extracellular component that is essential for the constitutive endocytic trafficking of
967 Notch in Drosophila. Development. 2007;134: 1347–1356. doi:10.1242/DEV.02811

968 69. Logeat F, Bessia C, Brou C, LeBail O, Jarriault S, Seidah NG, et al. The NOTCH1 receptor is cleaved
969 constitutively by a furin-like convertase. Proc Natl Acad Sci U S A. 1998;95: 8108–8112.
970 doi:10.1073/PNAS.95.14.8108

971 70. Goh JJH, Goh CJH, Lim QW, Zhang S, Koh CG, Chiam KH. Transcriptomics indicate nuclear division
972 and cell adhesion not recapitulated in MCF7 and MCF10A compared to luminal A breast tumours.
973 Scientific Reports 2022 12:1. 2022;12: 1–17. doi:10.1038/s41598-022-24511-z

974 71. Gross SM, Dane MA, Smith RL, Devlin KL, McLean IC, Derrick DS, et al. A multi-omic analysis of
975 MCF10A cells provides a resource for integrative assessment of ligand-mediated molecular and
976 phenotypic responses. Communications Biology 2022 5:1. 2022;5: 1–20. doi:10.1038/s42003-
977 022-03975-9

978 72. Saj A, Arziman Z, Stempfle D, van Belle W, Sauder U, Horn T, et al. A combined ex vivo and in vivo
979 RNAi screen for Notch regulators in Drosophila reveals an extensive Notch interaction network.
980 Dev Cell. 2010;18: 862–876. doi:10.1016/j.devcel.2010.03.013

981 73. Mummery-Widmer JL, Yamazaki M, Stoeger T, Novatchkova M, Bhalerao S, Chen D, et al.
982 Genome-wide analysis of Notch signalling in Drosophila by transgenic RNAi. Nature. 2009;458:
983 987–992. doi:10.1038/nature07936

984 74. Kankel MW, Hurlbut GD, Upadhyay G, Yajnik V, Yedvobnick B, Artavanis-tsakonas S. Investigating
985 the Genetic Circuitry of Mastermind in Drosophila, a Notch Signal Effector. 2007;2505: 2493–
986 2505. doi:10.1534/genetics.107.080994

987 75. Ho DM, Pallavi SK, Artavanis-tsakonas S. The Notch-mediated hyperplasia circuitry in Drosophila
988 reveals a Src-JNK signaling axis. 2015; 1–21. doi:10.7554/eLife.05996

989 76. Roti G, Carlton A, Ross KN, Markstein M, Pajcini K, Su AH, et al. Complementary genomic screens
990 identify SERCA as a therapeutic target in NOTCH1 mutated cancer. Cancer Cell. 2013;23: 390–
991 405. doi:10.1016/j.ccr.2013.01.015

992 77. Krämer A, Mentrup T, Kleizen B, Rivera-Milla E, Reichenbach D, Enzensperger C, et al. Small
993 molecules intercept Notch signaling and the early secretory pathway. Nat Chem Biol. 2013;9:
994 731–738. doi:10.1038/nchembio.1356

995 78. Shen CH, Chou CC, Lai TY, Hsu JE, Lin YS, Liu HY, et al. ZNRF1 Mediates Epidermal Growth Factor
996 Receptor Ubiquitination to Control Receptor Lysosomal Trafficking and Degradation. Front Cell
997 Dev Biol. 2021;9: 1103. doi:10.3389/FCELL.2021.642625/BIBTEX

998 79. Hoxhaj G, Caddye E, Najafov A, Houde VP, Johnson C, Dissanayake K, et al. The E3 ubiquitin ligase
999 ZNRF2 is a substrate of mTORC1 and regulates its activation by amino acids. Elife. 2016;5: 1–18.
1000 doi:10.7554/eLife.12278

1001 80. Sethna S, Scott PA, Giese APJ, Duncan T, Jian X, Riazuddin S, et al. CIB2 regulates mTORC1
1002 signaling and is essential for autophagy and visual function. Nature Communications 2021 12:1.
1003 2021;12: 1–19. doi:10.1038/s41467-021-24056-1

1004 81. Sanz-Castillo B, Hurtado B, Vara-Ciruelos D, el Bakkali A, Hermida D, Salvador-Barbero B, et al.
1005 The MASTL/PP2A cell cycle kinase-phosphatase module restrains PI3K-Akt activity in an mTORC1-
1006 dependent manner. EMBO J. 2023;42. doi:10.15252/EMBJ.2022110833

1007 82. Fatima I, Barman S, Uppada JP, Chauhan S, Rauth S, Rachagani S, et al. MASTL regulates EGFR
1008 signaling to impact pancreatic cancer progression. Oncogene. 2021;40: 5691–5704.
1009 doi:10.1038/S41388-021-01951-X

1010 83. Montero-Melendez T, Nagano A, Chelala C, Filer A, Buckley CD, Perretti M. Therapeutic
1011 senescence via GPCR activation in synovial fibroblasts facilitates resolution of arthritis. Nature
1012 Communications 2020 11:1. 2020;11: 1–15. doi:10.1038/s41467-020-14421-x

1013 84. Wang H, Huang F, Zhang Z, Wang P, Luo Y, Li H, et al. Feedback Activation of SGK3 and AKT
1014 Contributes to Rapamycin Resistance by Reactivating mTORC1/4EBP1 Axis via TSC2 in Breast
1015 Cancer. Int J Biol Sci. 2019;15: 929–941. doi:10.7150/IJBS.32489

1016 85. Chivukula I v., Ramsköld D, Storvall H, Anderberg C, Jin S, Mamaeva V, et al. Decoding breast
1017 cancer tissue-stroma interactions using species-specific sequencing. Breast Cancer Research.
1018 2015;17: 1–14. doi:10.1186/S13058-015-0616-X/FIGURES/4

1019 86. Nicolas M, Wolfer A, Raj K, Kummer JA, Mill P, van Noort M, et al. NOTCH1 functions as a tumor
1020 suppressor in mouse skin. Nat Genet. 2003;33: 416–21. doi:10.1038/ng1099

1021 87. Gosney JA, Wilkey DW, Merchant ML, Ceresa BP. Proteomics reveals novel protein associations
1022 with early endosomes in an epidermal growth factor- dependent manner. Journal of Biological
1023 Chemistry. 2018;293: 5895–5908. doi:10.1074/jbc.RA117.000632

1024 88. Miura GI, Roignant J, Wassef M, Treisman JE. Myopic acts in the endocytic pathway to enhance
1025 signaling by the Drosophila EGF receptor. Development. 2008;135: 1913–1922.
1026 doi:10.1242/dev.017202

1027 89. Ali N, Zhang L, Taylor S, Mironov A. Article Recruitment of UBPY and ESCRT Exchange Drive HD-
1028 PTP-Dependent Sorting of EGFR to the MVB. 2013; 453–461. doi:10.1016/j.cub.2013.02.033

1029 90. Moberg KH, Schelble S, Burdick SK, Hariharan IK. Mutations in erupted, the Drosophila ortholog
1030 of mammalian tumor susceptibility gene 101, elicit non-cell-autonomous overgrowth. Dev Cell.
1031 2005;9: 699–710. doi:10.1016/j.devcel.2005.09.018

1032 91. Manteghi S, Gingras MC, Kharitidi D, Galarneau L, Marques M, Yan M, et al. Haploinsufficiency of
1033 the ESCRT Component HD-PTP Predisposes to Cancer. Cell Rep. 2016;15: 1893–1900.
1034 doi:10.1016/J.CELREP.2016.04.076

1035 92. Lin G, Aranda V, Muthuswamy SK, Tonks NK. Identification of PTPN23 as a novel regulator of cell
1036 invasion in mammary epithelial cells from a loss-of-function screen of the 'PTP-ome''.' Genes
1037 Dev. 2011;25: 1412–1425. doi:10.1101/GAD.2018911

1038 93. Gugger M, Reubi JC. Gastrin-Releasing Peptide Receptors in Non-Neoplastic and Neoplastic
1039 Human Breast. Am J Pathol. 1999;155: 2067–2076. doi:10.1016/S0002-9440(10)65525-3

1040 94. Körner M, Waser B, Rehmann R, Reubi JC. Early over-expression of GRP receptors in prostatic
1041 carcinogenesis. Prostate. 2014;74: 217–224. doi:10.1002/PROS.22743

1042 95. Kato A, Kondo N, Wanifuchi-Endo Y, Fujita T, Asano T, Hisada T, et al. Low TINAGL1 expression is
1043 a marker for poor prognosis in breast cancer. J Cancer Res Clin Oncol. 2022 [cited 23 Feb 2023].
1044 doi:10.1007/S00432-022-04394-3

1045 96. Shen M, Jiang YZ, Wei Y, Ell B, Sheng X, Esposito M, et al. Tinagl1 Suppresses Triple-Negative
1046 Breast Cancer Progression and Metastasis by Simultaneously Inhibiting Integrin/FAK and EGFR
1047 Signaling. Cancer Cell. 2019;35: 64-80.e7. doi:10.1016/J.CCELL.2018.11.016

1048 97. Zhang H, Zhang LQ, Yang CC, Li J, Tian XY, Li DN, et al. The high expression of NUDT5 indicates
1049 poor prognosis of breast cancer by modulating AKT / Cyclin D signaling. PLoS One. 2021;16.
1050 doi:10.1371/JOURNAL.PONE.0245876

1051 98. Wright RHG, Lioutas A, Dily F le, Soronellas D, Pohl A, Bonet J, et al. ADP-ribose-derived nuclear
1052 ATP synthesis by NUDIX5 is required for chromatin remodeling. Science. 2016;352: 1221–1225.
1053 doi:10.1126/SCIENCE.AAD9335

1054 99. Sakurai T, Kamakura S, Hayase J, Kohda A, Nakamura M, Sumimoto H. GPR125 (ADGRA3) is an
1055 autocleavable adhesion GPCR that traffics with Dlg1 to the basolateral membrane and regulates
1056 epithelial apicobasal polarity. J Biol Chem. 2022;298. doi:10.1016/J.JBC.2022.102475

1057 100. Spina E, Simundza J, Incassati A, Chandramouli A, Kugler MC, Lin Z, et al. Gpr125 is a unifying
1058 hallmark of multiple mammary progenitors coupled to tumor latency. Nature Communications
1059 2022 13:1. 2022;13: 1–17. doi:10.1038/s41467-022-28937-x

1060 101. Xu K, Usary J, Kousis PC, Prat A, Wang DY, Adams JR, et al. Lunatic fringe deficiency cooperates
1061 with the Met/Caveolin gene amplicon to induce basal-like breast cancer. Cancer Cell. 2012;21:
1062 626–641. doi:10.1016/J.CCR.2012.03.041

1063 102. Zhang S, Chung WC, Miele L, Xu K. Targeting Met and Notch in the Lfng-deficient, Met-amplified
1064 triple-negative breast cancer. Cancer Biol Ther. 2014;15: 633–642. doi:10.4161/CBT.28180

1065 103. Huang KH, Sung IC, Fang WL, Chi CW, Yeh TS, Lee HC, et al. Correlation between HGF/c-Met and
1066 NOTCH1 signaling pathways in human gastric cancer cells. Oncol Rep. 2018;40: 294–302.
1067 doi:10.3892/OR.2018.6447

1068 104. Gude NA, Emmanuel G, Wu W, Cottage CT, Fischer K, Quijada P, et al. Activation of Notch-
1069 mediated protective signaling in the myocardium. Circ Res. 2008;102: 1025–1035.
1070 doi:10.1161/CIRCRESAHA.107.164749

1071 105. Stella MC, Trusolino L, Pennacchietti S, Comoglio PM. Negative feedback regulation of Met-
1072 dependent invasive growth by Notch. Mol Cell Biol. 2005;25: 3982–3996.
1073 doi:10.1128/MCB.25.10.3982-3996.2005

1074 106. Yang YF, Wang YY, Hsiao M, Lo S, Chang YC, Jan YH, et al. IMPAD1 functions as mitochondrial
1075 electron transport inhibitor that prevents ROS production and promotes lung cancer metastasis
1076 through the AMPK-NOTCH1-HEY1 pathway. Cancer Lett. 2020;485: 27–37.
1077 doi:10.1016/J.CANLET.2020.04.025

1078 107. Wu W, Sun XH. A mechanism underlying NOTCH-induced and ubiquitin-mediated JAK3
1079 degradation. J Biol Chem. 2011;286: 41153–41162. doi:10.1074/JBC.M111.273755

1080 108. Na J, Shin JY, Jeong H, Lee JY, Kim BJ, Kim WS, et al. JMJD3 and NF-κB-dependent activation of
1081 NOTCH1 gene is required for keratinocyte migration during skin wound healing. Sci Rep. 2017;7.
1082 doi:10.1038/S41598-017-06750-7

1083 109. Cordier C, Prevarskaya N, Lehen'kyi V. TRPM7 Ion Channel: Oncogenic Roles and Therapeutic
1084 Potential in Breast Cancer. Cancers (Basel). 2021;13. doi:10.3390/CANCERS13246322

1085 110. Liu M, Inoue K, Leng T, Guo S, Xiong Z gang. TRPM7 channels regulate glioma stem cell through
1086 STAT3 and Notch signaling pathways. Cell Signal. 2014;26: 2773.
1087 doi:10.1016/J.CELLSIG.2014.08.020

1088 111. Wan J, Guo AA, King P, Guo S, Saafir T, Jiang Y, et al. TRPM7 Induces Tumorigenesis and Stemness
1089 Through Notch Activation in Glioma. Front Pharmacol. 2020;11: 1.
1090 doi:10.3389/FPHAR.2020.590723/FULL

1091 112. Díaz-Tocados JM, Herencia C, Martínez-Moreno JM, Montes de Oca A, Rodríguez-Ortiz ME,
1092 Vergara N, et al. Magnesium Chloride promotes Osteogenesis through Notch signaling activation
1093 and expansion of Mesenchymal Stem Cells. Sci Rep. 2017;7. doi:10.1038/S41598-017-08379-Y

1094 113. Yan D, Jin Y. Regulation of DLK-1 kinase activity by calcium-mediated dissociation from an
1095 inhibitory isoform. Neuron. 2012;76: 534–548. doi:10.1016/J.NEURON.2012.08.043

1096 114. Tortosa E, Sengupta Ghosh A, Li Q, Wong WR, Hinkle T, Sandoval W, et al. Stress-induced
1097 vesicular assemblies of dual leucine zipper kinase are signaling hubs involved in kinase activation
1098 and neurodegeneration. EMBO J. 2022;41. doi:10.15252/EMBJ.2021110155

1099 115. Ko SH, Apple EC, Liu Z, Chen L. Age-dependent autophagy induction after injury promotes axon
1100 regeneration by limiting NOTCH. Autophagy. 2020;16: 2052.
1101 doi:10.1080/15548627.2020.1713645

1102 116. Mamaeva OA, Kim J, Feng G, McDonald JM. Calcium/calmodulin-dependent kinase II regulates
1103 notch-1 signaling in prostate cancer cells. J Cell Biochem. 2009;106: 25–32.
1104 doi:10.1002/JCB.21973

1105 117. Choi YH, Ann EJ, Yoon JH, Mo JS, Kim MY, Park HS. Calcium/calmodulin-dependent protein kinase
1106 IV (CaMKIV) enhances osteoclast differentiation via the up-regulation of NOTCH1 protein
1107 stability. Biochim Biophys Acta. 2013;1833: 69–79. doi:10.1016/J.BBAMCR.2012.10.018

1108 118. Qu J, Zhou Y, Li Y, Yu J, Wang W. CASK regulates Notch pathway and functions as a tumor
1109 promoter in pancreatic cancer. Arch Biochem Biophys. 2021;701.
1110 doi:10.1016/J.ABB.2021.108789

1111 119. Chakravarti B, Yang J, Ahlers-Dannen KE, Luo Z, Flaherty HA, Meyerholz DK, et al. Essentiality of
1112 Regulator of G Protein Signaling 6 and Oxidized Ca2+/Calmodulin-Dependent Protein Kinase II in
1113 Notch Signaling and Cardiovascular Development. J Am Heart Assoc. 2017;6.
1114 doi:10.1161/JAHA.117.007038

1115 120. Mok K, Tsoi H, Man EP, Leung M, Chau KM, Wong L, et al. Repurposing hyperpolarization-
1116 activated cyclic nucleotide-gated channels as a novel therapy for breast cancer. Clin Transl Med.
1117 2021;11: 11. doi:10.1002/CTM2.578

1118 121. Giuli M v., Giuliani E, Screpanti I, Bellavia D, Checquolo S. Notch Signaling Activation as a Hallmark
1119 for Triple-Negative Breast Cancer Subtype. J Oncol. 2019;2019. doi:10.1155/2019/8707053

1120 122. Endo A, Matsumoto M, Inada T, Yamamoto A, Nakayama KI, Kitamura N, et al. Nucleolar
1121 structure and function are regulated by the deubiquitylating enzyme USP36. J Cell Sci. 2009;122:
1122 678–686. doi:10.1242/JCS.044461

1123 123. Wang W, Lei Y, Zhang G, Li X, Yuan J, Li T, et al. USP39 stabilizes β-catenin by deubiquitination
1124 and suppressing E3 ligase TRIM26 pre-mRNA maturation to promote HCC progression. Cell Death
1125 Dis. 2023;14. doi:10.1038/S41419-023-05593-7

1126 124. Havugimana PC, Hart GT, Nepusz T, Yang H, Turinsky AL, Li Z, et al. A Census of Human Soluble
1127 Protein Complexes. Cell. 2012;150: 1068. doi:10.1016/J.CELL.2012.08.011

1128 125. Sun XX, He X, Yin L, Komada M, Sears RC, Dai MS. The nucleolar ubiquitin-specific protease USP36
1129 deubiquitinates and stabilizes c-Myc. Proc Natl Acad Sci U S A. 2015;112: 3734–3739.
1130 doi:10.1073/PNAS.1411713112

1131 126. Fraile JM, Campos-Iglesias D, Rodríguez F, Astudillo A, Vilarrasa-Blasi R, Verdaguer-Dot N, et al.
1132 Loss of the deubiquitinase USP36 destabilizes the RNA helicase DHX33 and causes
1133 preimplantation lethality in mice. J Biol Chem. 2018;293: 2183–2194.
1134 doi:10.1074/JBC.M117.788430

1135 127. Taillebourg E, Gregoire I, Viargues P, Jacomin AC, Thevenon D, Faure M, et al. The
1136 deubiquitinating enzyme USP36 controls selective autophagy activation by ubiquitinated
1137 proteins. Autophagy. 2012;8: 767–779. doi:10.4161/AUTO.19381

1138 128. Buszczak M, Paterno S, Spradling AC. Drosophila stem cells share a common requirement for the
1139 histone H2B ubiquitin protease scrawny. Science (1979). 2009;323: 248–251.
1140 doi:10.1126/SCIENCE.1165678/SUPPL_FILE/BUSZCZAK_SOM.PDF

1141
1142

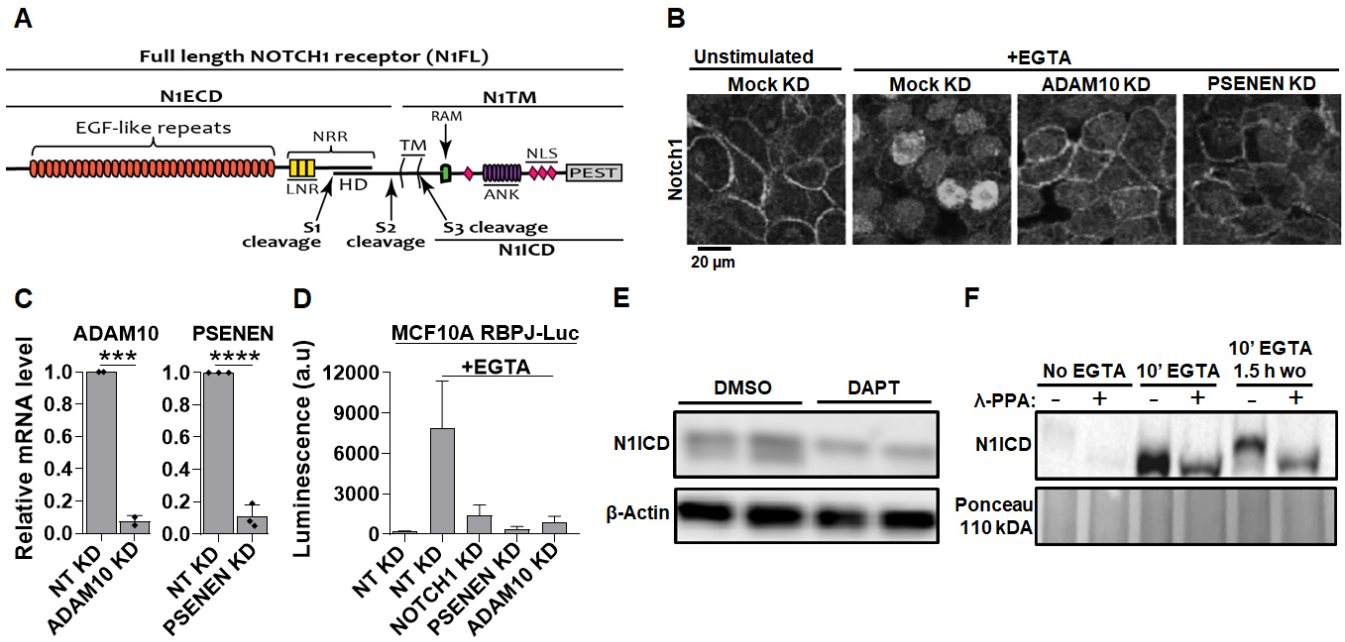

Fig. 1: Manipulation of endogenous NOTCH1 signaling in MCF10A cells. **(A)** The NOTCH1 (N1) full length receptor (N1FL) is composed of the N1 extracellular domain (N1ECD) and of the N1 transmembrane domain (N1TM). The N1ECD contains several EGF-like repeats, some of which are binding sites for Notch ligands as well as the negative regulatory region (NRR), which includes the Lin12/Notch Repeats (LNR) and the heterodimerization domain (HD). The N1ICD and N1ECD portions of Notch receptors are produced by Furin cleavage occurring at the S1 site during trafficking to the trans-Golgi network (TGN). N1ICD and N1ECD are non-covalently held together by Ca^{2+} at the HD. Ca^{2+} depletion causes ADAM10 and γ-secretase to sequentially cleave the receptor at S2 and S3 sites. This leads to the release in the cytoplasm of the N1 intracellular domain (N1ICD), which translocates to the nucleus. N1ICD contains the RBP-J-kappa-associated module (RAM), ankyrin repeats (ANK), nuclear localization signals (NLS), and the proline (P), glutamic acid (E), serine (S) and threonine (T) – PEST domain, which limits NICD half-life. **(B)** Immunofluorescence reveals that EGTA treatment relocates most endogenous NOTCH1 from the cell surface to the nucleus and this is inhibited by silencing *ADAM10* or *PSENEN*. **(C)** siRNA against *ADAM10* or *PSENEN* effectively deplete their mRNA. **(D)** The Notch reporter cell line, MCF10A-RbpJk-Luc, reports strong EGTA-induced Notch signaling, and this effect is markedly suppressed by silencing *NOTCH1, PSENEN* or *ADAM10*. **(E)** Western blot analysis of MCF10A cell extracts using an antibody against S3-cleaved N1 shows that unstimulated cells express low levels of N1ICD, which appears as a doublet. γ-secretase inhibition for 3 hours (DAPT) markedly reduces basal levels of the N1ICD lower band. **(F)** Western blot analysis of MCF10A lysates indicates that λ-phosphatase (λ-PPA) treatment leads to disappearance of the upper band of the N1ICD doublet, indicating that it corresponds to a phosphorylated N1CD form. *** and **** indicate $p < 0.001$ and $p < 0.0001$, respectively.

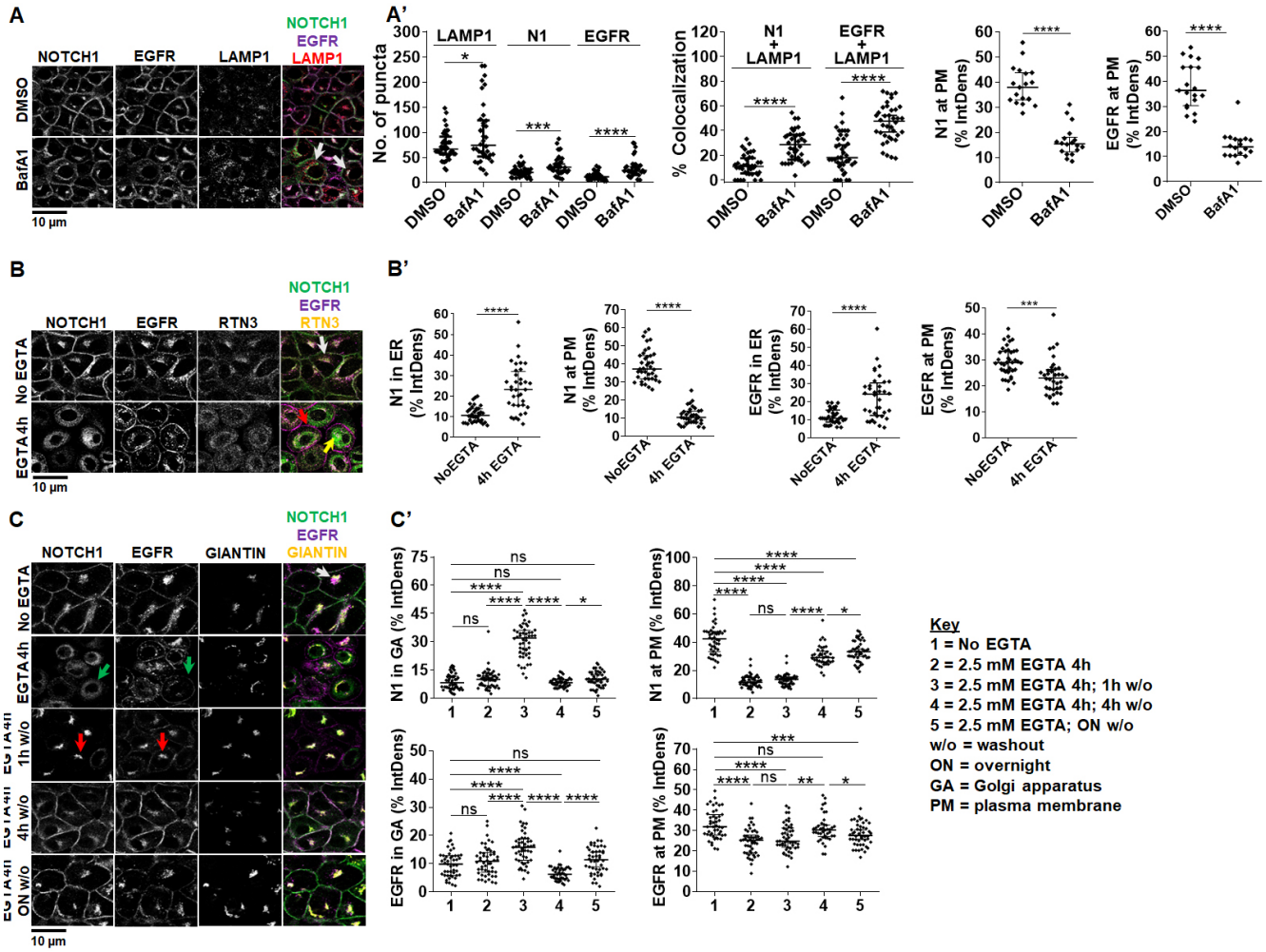

Fig. 2: Endocytic and exocytic endogenous NOTCH1 receptor trafficking in MCF10A cells. **(A)** Confocal sections of MCF10A cells treated and immunolabeled as indicated. Upon BafA1 treatment, plasma membrane (PM) localization of both NOTCH1 and EGFR is reduced and both receptors accumulate in LAMP1-positive compartments (arrows; quantified in A'). (**B**) Confocal sections of MCF10A cells treated and immunolabeled as indicated. 4-hour EGTA treatment depletes NOTCH1 from the PM and strongly accumulates it in a RTN3-positive compartment (yellow arrow), whereas EGFR remains on the PM (red arrow). In unstimulated cells, a pool of both NOTCH1 and EGFR is visible in the RTN3-positive compartment (white arrow). **(C)** Confocal sections of MCF10A cells treated and immunolabeled as indicated. An intracellular pool of NOTCH1 and EGFR colocalizes with the Golgi apparatus (GA) marker, GIANTIN (white arrow). Compared with non-EGTA treated cells, 4-hour EGTA treatment causes diffused NOTCH1 and EGFR accumulation in the cytosol, with some EGFR remaining on the PM (green arrows). The Giantin signal is also diffused consistent with an expected fragmentation of the GA. EGTA washout (w/o) for 1 hour causes all NOTCH1 and most EGFR signal to localize in the GA (red arrows). EGTA w/o for 4 hours or overnight (ON) restores normal intracellular distribution of NOTCH1 and EGFR (quantified in C'; *, **, ***, ****, ns indicate $p < 0.05$, $p < 0.01$, $p < 0.001$, $p < 0.0001$, and not significant, respectively).

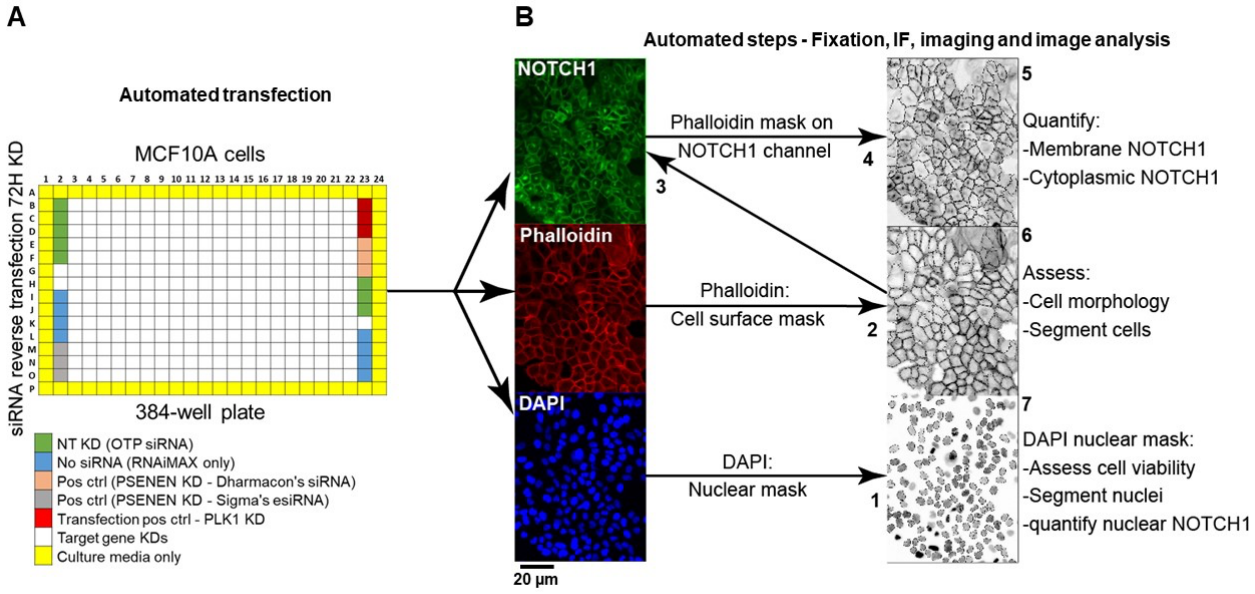

Fig. 3: High content screen pipeline and image analysis strategy. **(A)** The primary screen was performed on MCF10-A cells in a 384-well format. Genes belonging to a subset of the human genome, were knocked down in 6 replicate plates for 72 hours by RNAi along with the listed controls. In a duplicate experiment, cells were stimulated with EGTA. Control wells were distributed in the plates as shown. NT: non-targeting KD – cells were transfected with non-targeting siRNA. No siRNA: cells received RNAiMAX only. Pos ctrl (positive control) – cells were transfected with siRNA against *PSENEN*. Transfection pos ctrl: cells were transfected with siRNA against *PLK1* (Polo-like kinase 1) as a cytotoxic indicator of transfection efficiency. Outer wells (yellow) were filled with media to prevent evaporation in experimental wells. **(B)** To assess endogenous NOTCH1 localization, cells in plates were subjected to automated IF and DAPI/phalloidin labeling to demarcate nuclei and the cell cortex, respectively. The script steps of the image acquisition and analysis developed in-house are as follows: (1) The nuclei were segmented based on DAPI signal. (2) The cell surface was segmented using the phalloidin signal and overlaid on the NOTCH1 channel (3) to quantify levels of cell surface NOTCH1 (4) and the area between the cell cortex and the nuclei was used to determine levels of cytoplasmic NOTCH1 (5). (6) The phalloidin mask was also used to count cells and establish cell-to-cell boundaries. (7) Nuclear size was used as a readout of cell viability as compact, pycnotic nuclei identify dead cells. Using such a pipeline, each gene KD was defined by its effects on the amount of NOTCH1 at the cell cortex, in the cytoplasm or in the nucleus.

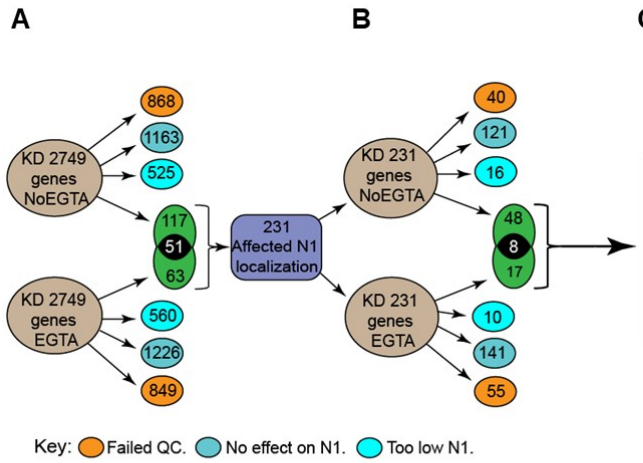

Effect upon KD relative to NT KD	No. of Hits
Increased cytoplasmic N1 localization in NoEGTA	36
Increased cytoplasmic N1 localization in +EGTA	8
Increased total (whole cell) N1 in NoEGTA	1
Reduced total (whole cell) N1	1
Elevated N1 in +EGTA only	5
Total	51

51 hits reproduced 1° screen phenotypes

Fig. 4: Schematics of the primary and secondary screens and of the candidate genes classification process. (A) A total of 2749 genes were silenced in the primary screen. Candidates that when compared with controls led to marked cytotoxicity, did not affect intracellular NOTCH1 (**N1**) localization, or caused general loss of NOTCH1 signal, were excluded from further analysis (orange, blue, and light blue circles, respectively). A total of 231 genes that altered intracellular NOTCH1 localization were identified (green). 117 did so in unstimulated condition, 63 upon EGTA stimulation and 51 in both conditions. **(B)** The 231 candidates underwent secondary screening. 73 of the 231 led to changes in NOTCH1 localization but only 51 genes reproduced the primary screen phenotypes. **(C)** Of these 51, 38 affected NOTCH1 trafficking in the unstimulated No EGTA condition, 13 altered NOTCH1 trafficking in the stimulated +EGTA condition.

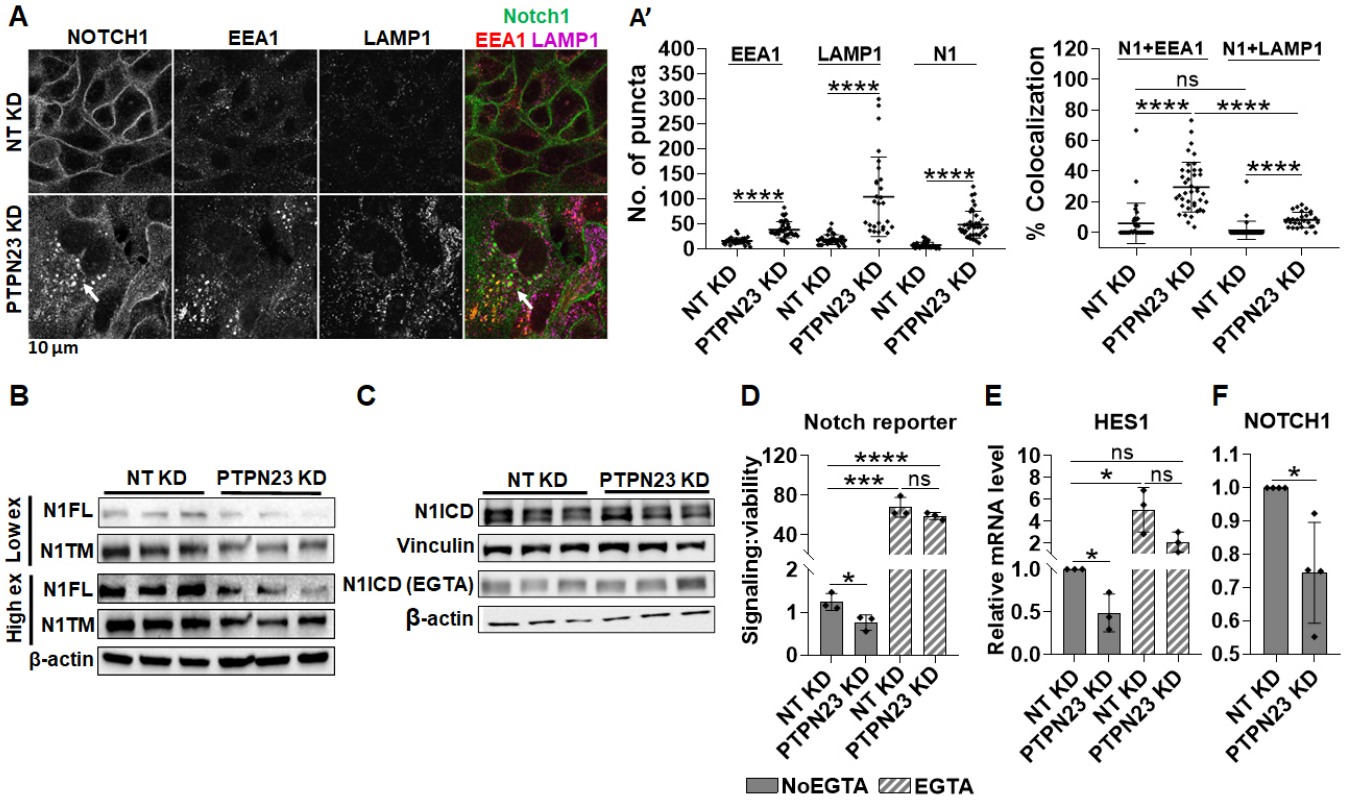

Fig. 5: Analysis of NOTCH1 localization and signaling activity upon *PTPN23* silencing. (A) Confocal sections of MCF10A cells treated and immunolabeled as indicated. *PTPN23* silencing causes marked increase in the number of EEA1, LAMP1, and NOTCH1 (N1) puncta, as well as accumulation of intracellular NOTCH1 positive puncta, which mostly colocalize with EEA1 (arrows; quantified in A'). **(B–C)** Western blot analyses indicate that *PTPN23* depletion reduces the levels of N1FL and N1TM but does not alter N1ICD levels with or without EGTA. Note that levels of N1ICD in unstimulated and EGTA stimulated cells are not comparable in C, due to different detection methods (see materials and methods). **(D-F)** The Notch reporter cell line MCF10A-RbpJk-Luc and RT-qPCR analysis reveal that *PTPN23* depletion suppresses basal Notch signaling. *, ***, ****, and ns indicates $p < 0.05$, $p < 0.001$, $p < 0.0001$, and not significant, respectively.

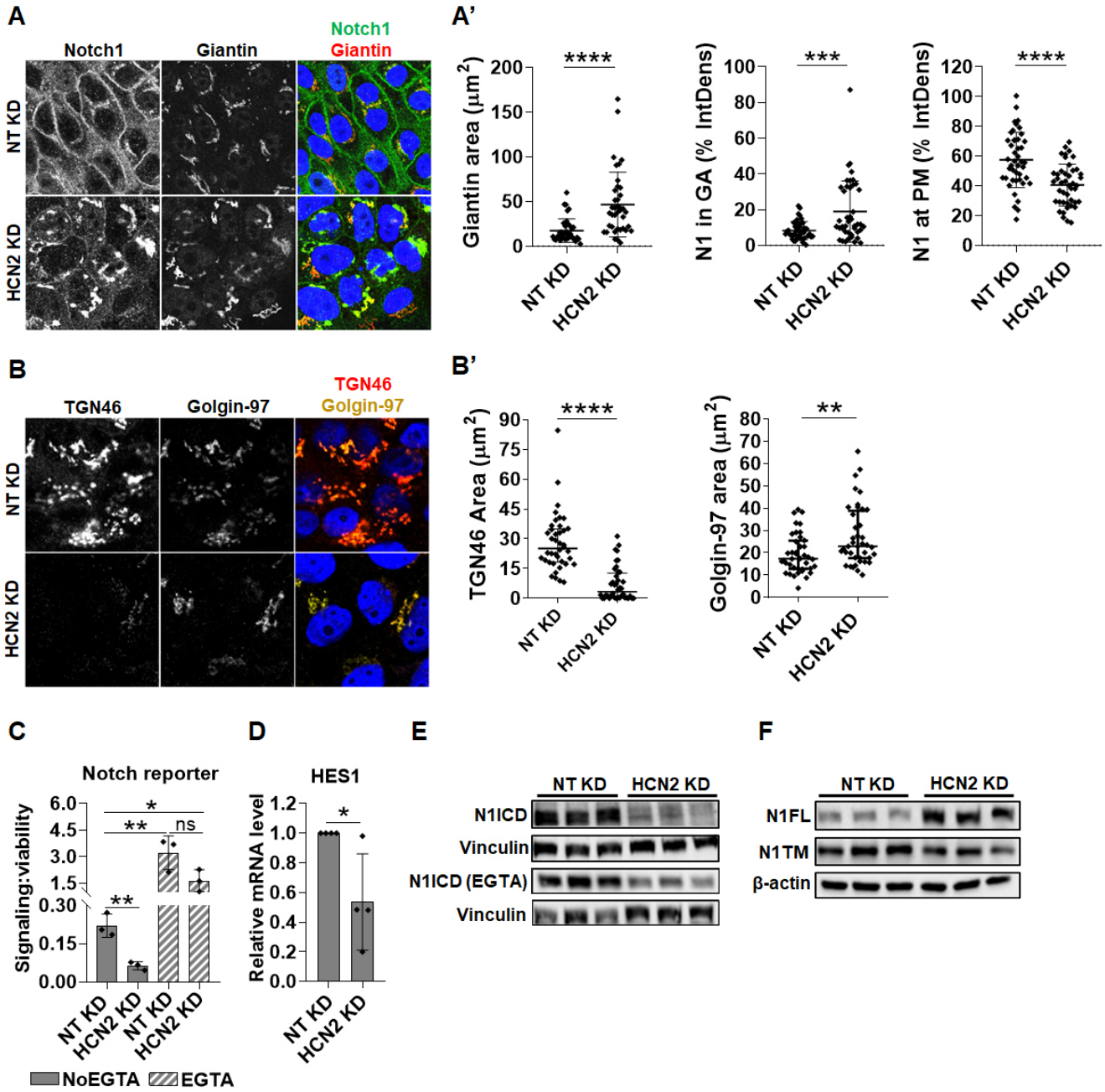

Fig. 6: Analysis of NOTCH1 localization and signaling activity upon *HCN2* silencing. (A) Confocal sections of MCF10A cells treated and immunolabeled as indicated. *HCN2* silencing causes marked NOTCH1 accumulation in the Giantin-positive compartment while significantly reducing cell surface NOTCH1 (N1) levels (quantified in A'). **(B)** Confocal sections of MCF10A cells treated and immunolabeled as indicated. *HCN2* silencing markedly depletes the TGN46-positive TGN compartment but not the Golgin-97-positive TGN compartment (quantified in B'). **(C–D)** The Notch reporter cell line, MCF10A-RbpJk-Luc and RT-qPCR analysis reveal that *HCN2* silencing suppresses basal Notch signaling. **(E)** Western blot analyses indicate that *HCN2* depletion reduces both basal and EGTA-stimulated N1ICD levels. Note that levels of N1ICD in unstimulated and EGTA stimulated cells are not comparable in C, due to different detection methods (see materials and methods). **(F)** Western blot analysis indicates that *HCN2* silencing results in marked accumulation of N1FL. *, **, ****, and ns indicate $p < 0.05$, $p < 0.01$, $p < 0.0001$, and not significant, respectively.

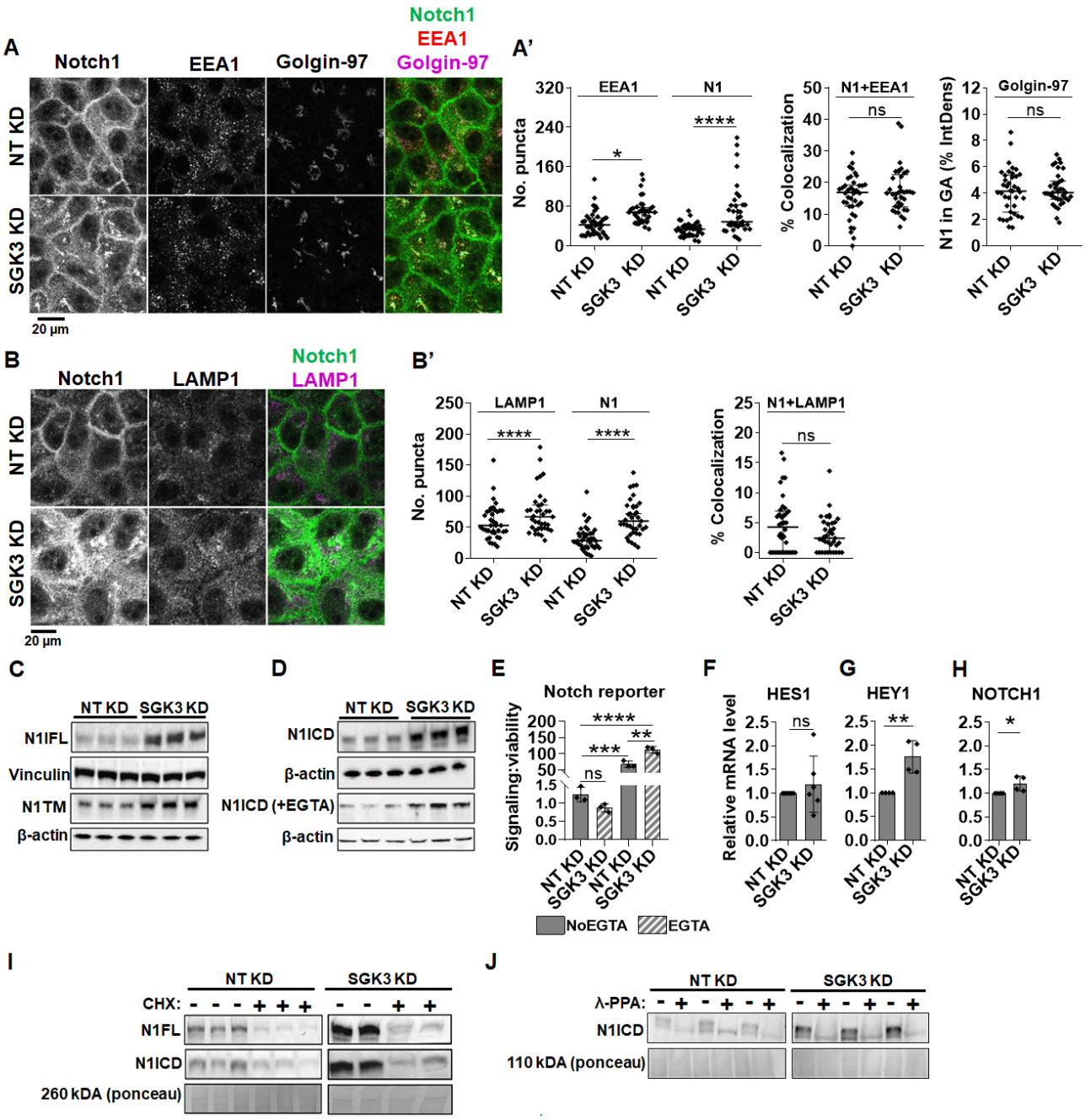

Fig. 7: Analysis of NOTCH1 localization and signaling activity upon *SGK3* silencing. (A) Confocal sections of MCF10A cells treated and immunolabeled as indicated. *SGK3* silencing causes NOTCH1 (N1) accumulation in the cytoplasm without apparent co-localization with EEA1 or Golgin-97 (quantified in A'). **(B)** Confocal sections of MCF10A cells treated and immunolabeled as indicated. The accumulated N1 upon *SGK3* silencing does not colocalize with LAMP1 (quantified in B'). **(C–D)** Western blot analyses show that *SGK3* depletion causes strong accumulation of all forms of the NOTCH1 receptor. Note that levels of N1ICD in unstimulated and EGTA stimulated cells are not comparable in C, due to different detection methods (see materials and methods). **(E)** The Notch reporter cell line MCF10A-RbpJk-Luc reveals that *SGK3* silencing enhances Notch signaling in EGTA-stimulated cells. **(F–H)** RT-qPCR analysis reveals that *SGK3* depletion enhances basal expression of HEY1 and NOTCH1. **(I)** Western blot analyses indicate that SGK3 does not destabilize N1ICD or N1FL. **(J)** Western blot analyses of lysates treated with λ-phosphatase (λ-PPA) showed that similar to controls, most of the N1ICD that accumulates upon

SGK3 silencing is phosphorylated. *, **, ***, ****, and ns indicate p <0.05, p <0.01, p <0.001, p <0.0001, and not significant, respectively.

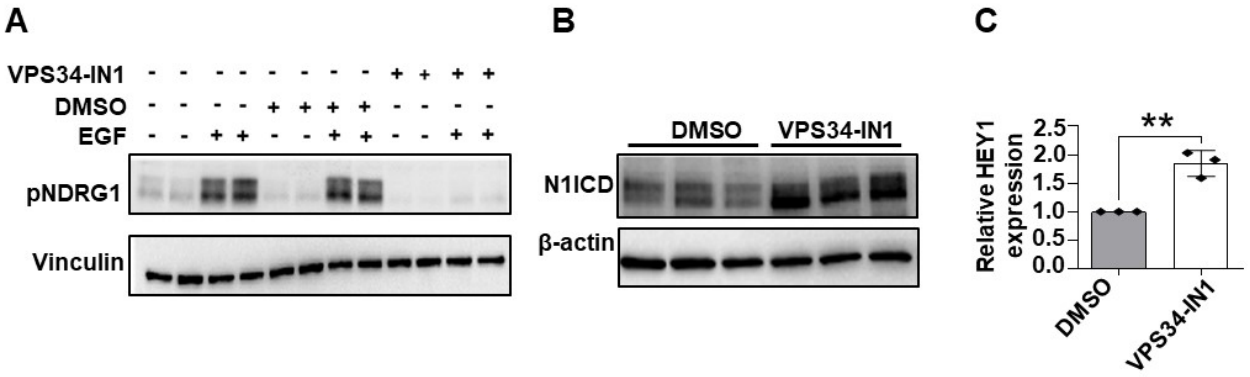

Fig. 8: Pharmacologic SGK3 inhibition elevates γ-secretase-derived N1ICD and Notch signaling. Western blot analysis reveals that serum-starved, VPS34-IN1-treated, MCF10A cells fail to phosphorylate the SGK3 target NDRG1 upon EGF treatment. **(B)** Western blot analysis reveals that pharmacologic VPS34-IN1 treatment enhances N1ICD levels. **(C)** RT-qPCR analysis shows that pharmacologic VPS34-IN1 treatment significantly enhances the expression of the Notch target gene HEY1. ** indicates p <0.01.

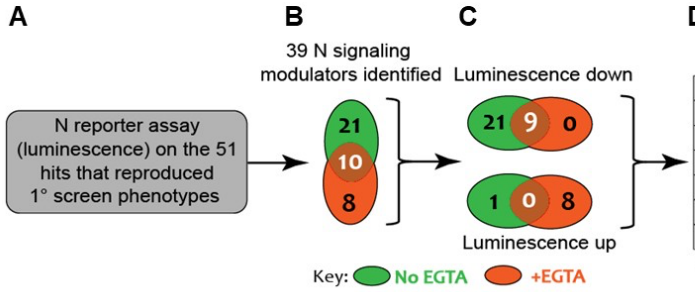

Effect upon KD relative to NT KD	No. of Hits
Increased cytoplasmic N1 localization in NoEGTA	25
Increased cytoplasmic N1 localization in +EGTA	8
Increased total (whole cell) N1 in NoEGTA	1
Reduced total (whole cell) N1	1
Elevated N1 in +EGTA only	4
Total	39

Phenotypic classes of the 39 N signaling modulators

Fig. 9: A secondary screen using a Notch reporter identifies 39 new signaling modulators. (A–B) MCF10A-RbpJk-Luc Notch reporter assay identifies 39 candidates that affect Notch signaling. **(C)** Of the 39, 30 suppress Notch signaling while 9 enhance Notch signaling. **(D)** Classification of the 39 candidates by their effect on intracellular NOTCH1 (N1) localization and/or levels.

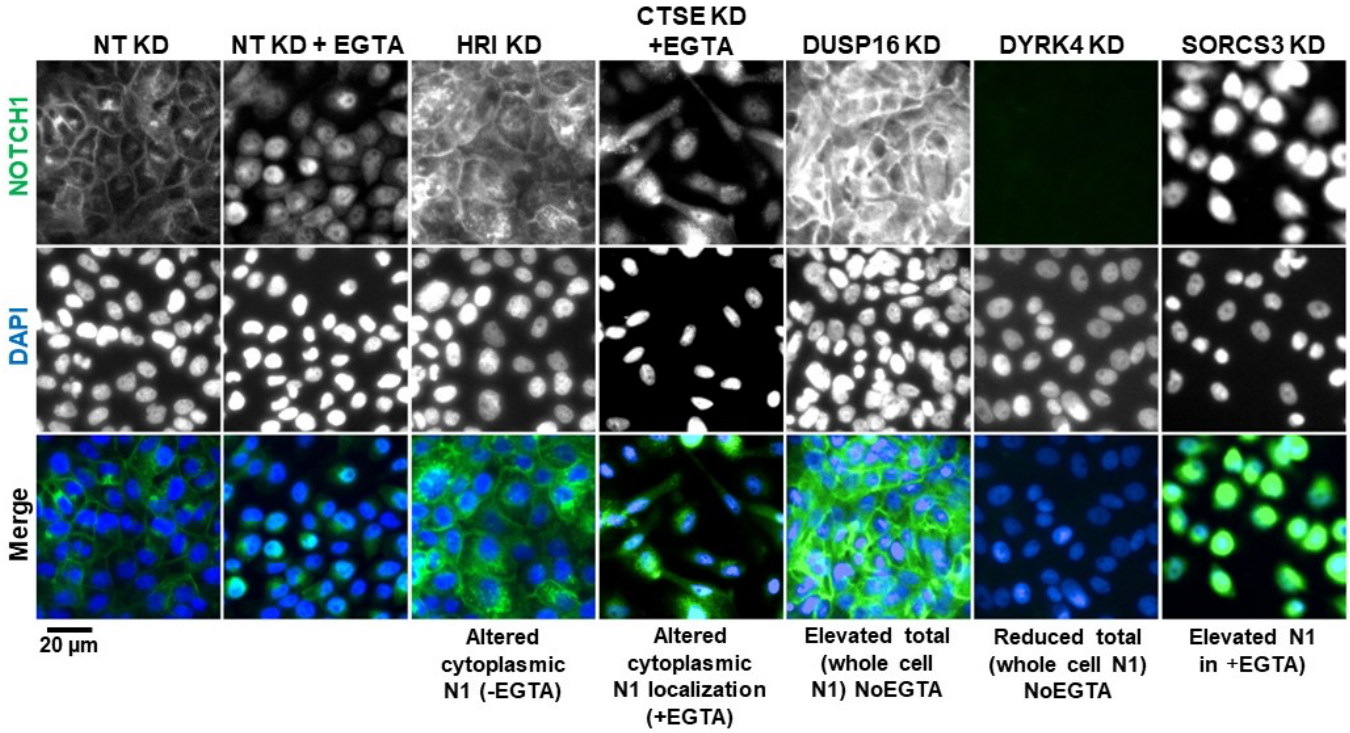

Supplemental Fig. 1: Representative images of the Notch phenotypic classes. High content screening (primary screen) widefield images of MCF10A cells treated and immunolabeled as indicated. Genes were grouped into the indicated classes based on their effect on intracellular NOTCH1 (N1) localization in NoEGTA or EGTA conditions.

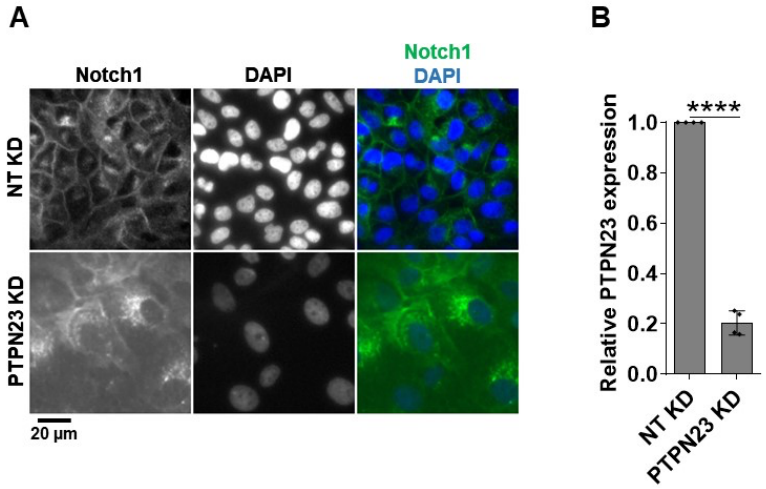

Supplemental Fig. 2: Effects of *PTPN23* silencing. (A) A high content screening widefield image of MCF10A cells treated and immunolabeled as indicated. *PTPN23* silencing causes marked accumulation of NOTCH1-positive puncta. **(B)** RT-qPCR analysis indicates effective *PTPN23* depletion. **** indicates $p < 0.0001$.

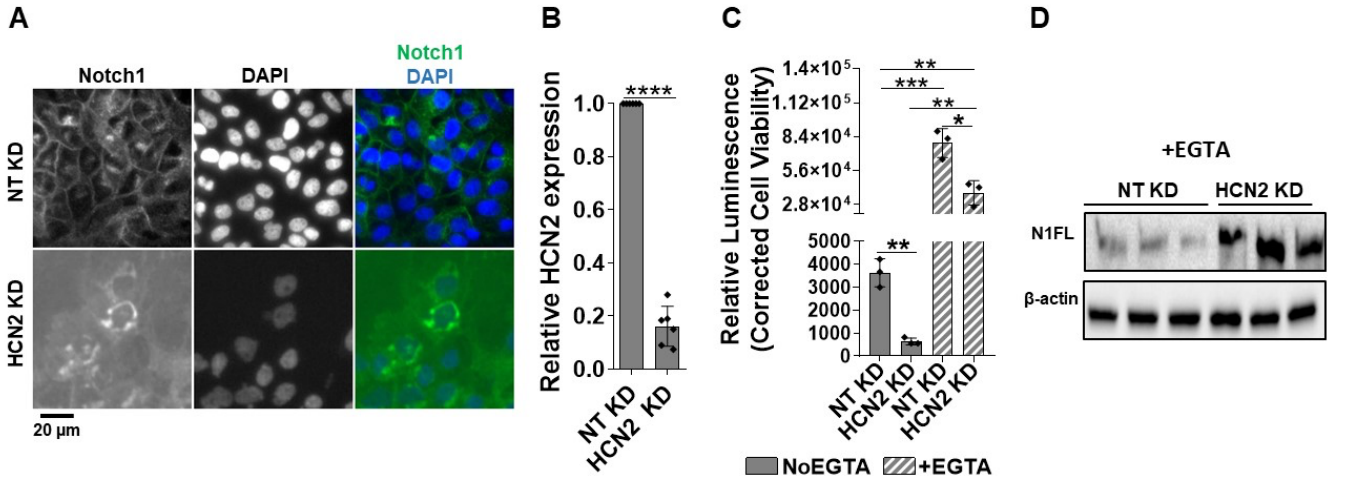

Supplemental Fig. 3: Effects of *HCN2* silencing. (A) A high content screening widefield image of MCF10A cells treated and immunolabeled as indicated. *HCN2* silencing causes marked NOTCH1 accumulation in the perinuclear region. **(B)** RT-qPCR analysis indicates effective *HCN2* depletion. **(C)** The Notch reporter cell line MCF10A-RbpJk-Luc reveals that *HCN2* silencing suppresses Notch signaling in No EGTA and EGTA conditions. **(D)** Western blot analysis indicates that *HCN2* silencing enhances N1FL levels in EGTA conditions. *, **, ***, and **** indicate p <0.05, p <0.01, p <0.001, and p <0.0001, respectively.

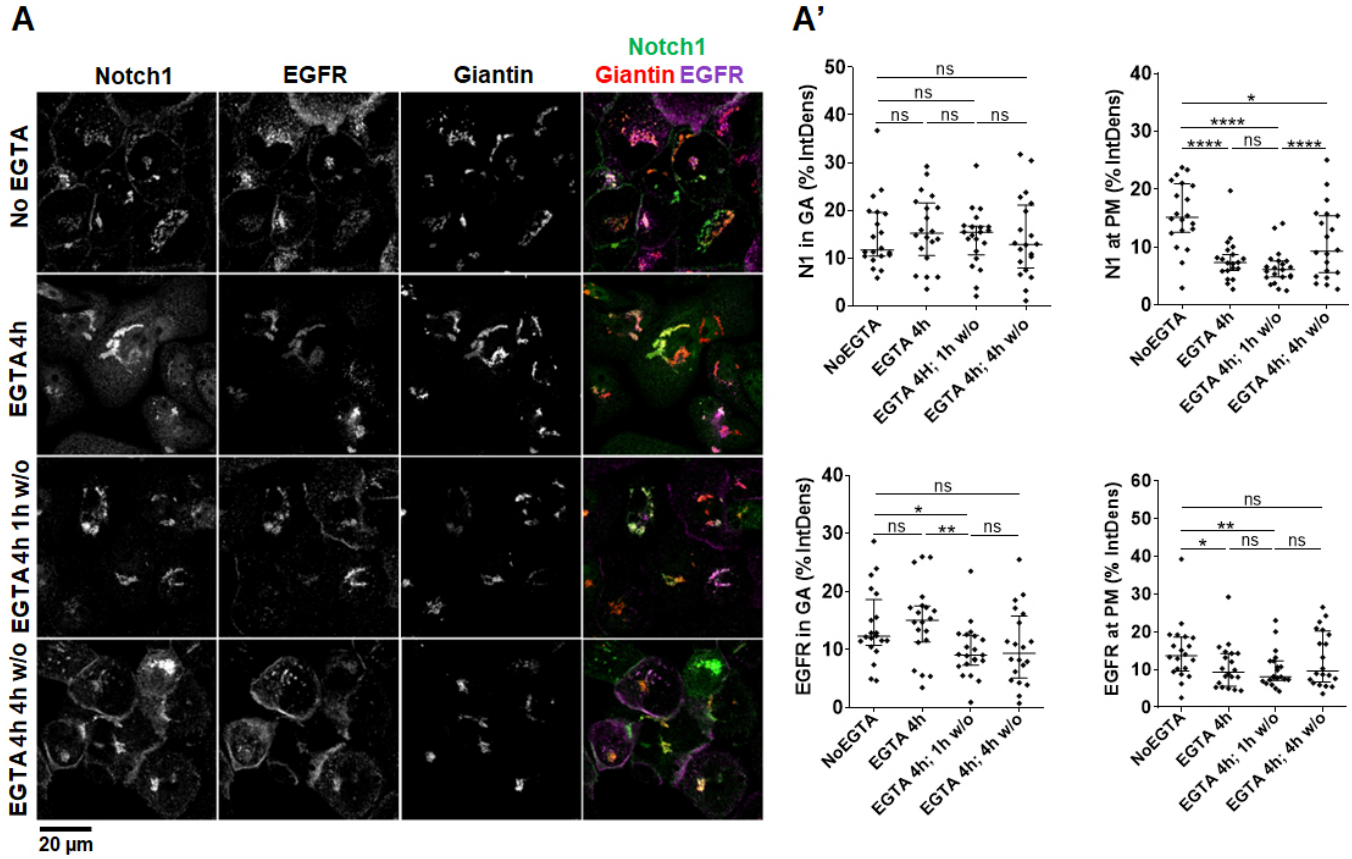

Supplemental Fig. 4: NOTCH1 secretion dynamics upon *HCN2* KD. (A) Confocal sections of MCF10A cells treated and immunolabeled as indicated. Quantification in A'; *, **, ****, and ns indicate p <0.05, p <0.01, p <0.0001, and not significant, respectively.

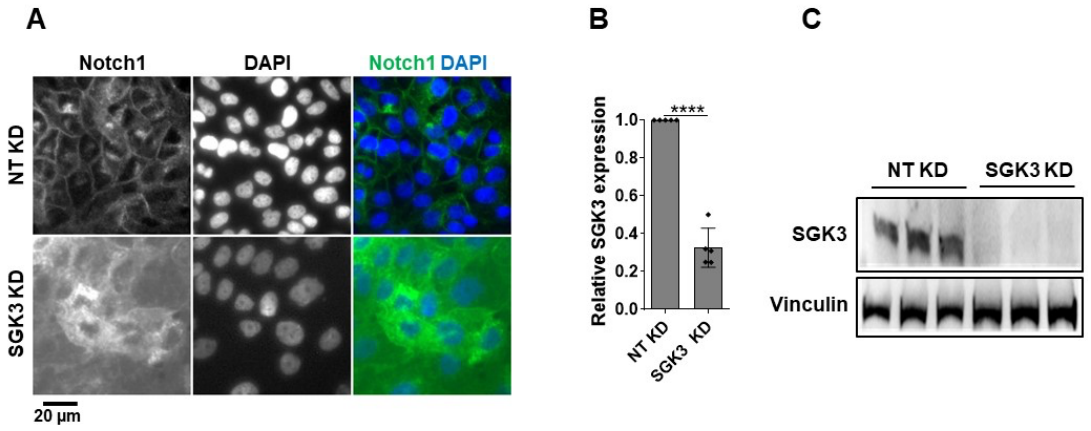

Supplemental Fig. 5: Effects of *SGK3* silencing. (A) A high content screening widefield image of MCF10A cells treated and immunolabeled as indicated. *SGK3* silencing causes marked NOTCH1 accumulation in the cytoplasm. **(B–C)** RT-qPCR and Western blot analyses indicate effective *SGK3* depletion. **** indicates $p < 0.0001$.